The FASEB Journal article fj.15-278739. Published online December 30, 2015.

The FASEB Journal • Research Communication

APP-dependent glial cell line-derived neurotrophic factor gene expression drives neuromuscular junction formation

Serena Stanga,* Nadège Zanou,† Emilie Audouard,‡ Bernadette Tasiaux,* Sabrina Contino,* Gaëlle Vandermeulen,§ Frédérique René,¶ Jean-Philippe Loeffler,¶ Frédéric Clotman,‡ Philippe Gailly,† Ilse Dewachter,* Jean-Noël Octave,* and Pascal Kienlen-Campard*,[1]

*Alzheimer Research Group, †Laboratory of Cell Physiology, and ‡Laboratory of Neural Differentiation, Institute of Neuroscience, and §Advanced Drug Delivery and Biomaterials, Louvain Drug Research Institute, Université Catholique de Louvain, Brussels, Belgium; and ¶Institut National de la Santé et de la Recherche Médicale, Unité 1118 Mécanismes Centraux et Périphériques de la Neurodégénérescence, Université de Strasbourg, Strasbourg Cedex, France

ABSTRACT **Besides its crucial role in the pathogenesis of Alzheimer's disease, the knowledge of amyloid precursor protein (APP) physiologic functions remains surprisingly scarce. Here, we show that APP regulates the transcription of the *glial cell line-derived neurotrophic factor* (*GDNF*). APP-dependent regulation of GDNF expression affects muscle strength, muscular trophy, and both neuronal and muscular differentiation fundamental for neuromuscular junction (NMJ) maturation *in vivo*. In a nerve–muscle coculture model set up to modelize NMJ formation *in vitro*, silencing of muscular APP induces a 30% decrease in secreted GDNF levels and a 40% decrease in the total number of NMJs together with a significant reduction in the density of acetylcholine vesicles at the presynaptic site and in neuronal maturation. These defects are rescued by GDNF expression in muscle cells in the conditions where muscular APP has been previously silenced. Expression of GDNF in muscles of amyloid precursor protein null mice corrected the aberrant synaptic morphology of NMJs. Our findings highlight for the first time that APP-dependent GDNF expression drives the process of NMJ formation, providing new insights into the link between APP gene regulatory network and physiologic functions.—Stanga, S., Zanou, N., Audouard, E., Tasiaux, B., Contino, S., Vandermeulen, G., René, F., Loeffler, J.-P., Clotman, F., Gailly, P., Dewachter, I., Octave, J.-N., Kienlen-Campard, P. APP-dependent glial cell line-derived neurotrophic factor gene expression drives neuromuscular junction formation. *FASEB J.* 30, 000–000 (2016). www.fasebj.org**

Key Words: gene transcription · Alzheimer's disease · APP knockout mice · nerve–muscle coculture · muscle electroporation

Identification of the amyloid precursor protein (APP) (1) raised a huge research effort aimed at understanding the mechanisms of β-amyloid peptide (Aβ) production and its pathologic role. Aβ is released by secretase-mediated proteolytic cleavage of APP (2); it is the major constituent of senile plaques found in Alzheimer's disease (AD) brains. Together with synaptic dysfunction and cognitive decline, progressive accumulation and deposition of Aβ are typical hallmarks of the disease. Apart from producing Aβ, a key player in AD pathogenesis, the role of the APP *per se* in physiopathologic pathways remains poorly understood.

APP belongs to a protein family formed by 3 paralogs in mammals: APP, and amyloid precursor-like proteins (APLPs) 1 and 2. APP and APLP2 are ubiquitously expressed, whereas APLP1 expression is mainly restricted to the nervous system (3).The different functions assigned to APP and its paralogs are not converging to a clearly defined model for APP family function and did not identify a concrete and specific role for each member (4). The picture becomes even more complex considering that 3 major isoforms of APP (APP695, APP751, and APP770) are generated as a result of alternative splicing. No conclusive functional differences have been ascribed to the different APP isoforms so far (4, 5). The physiologic functions of APP and the signaling pathways activated by APP remain scarcely understood. It has been reported that the secreted APP ectodomain (APPsα) restores by itself defects observed in amyloid precursor protein null ($APP^{-/-}$) mice (6), but other studies have suggested that the amyloid precursor protein intracellular domain (AICD) is required for APP functions, in agreement with the hypothesis that AICD-dependent gene transcription is essential in APP function (7, 8). The identity of the APP target genes

Abbreviations: βIIItub, βIII tubulin; Aβ, β-amyloid peptide; ACh, acetylcholine; AChR, acetylcholine receptor; AD, Alzheimer's disease; AICD, amyloid precursor protein intracellular domain; ALS, amyotrophic lateral sclerosis; APLP, amyloid precursor-like protein; APP, amyloid precursor protein; $APP^{-/-}$, amyloid precursor protein null; (*continued on next page*)

[1] Correspondence: Université Catholique de Louvain, Institute of Neuroscience IONS-CEMO, Avenue Mounier 53 bte B1.53.02, 1200 Brussels, Belgium. E-mail: pascal.kienlen-campard@uclouvain.be

doi: 10.1096/fj.15-278739

This article includes supplemental data. Please visit *http://www.fasebj.org* to obtain this information.

identified so far (9–11) remains a matter of debate. In addition, many of them appear not to be obviously linked to the phenotype observed in APP$^{-/-}$ mice.

APP$^{-/-}$ mice display a mild phenotype with decreased body and brain weight (12), along with reduced locomotor activity and grip strength (12, 13). A more detailed analysis of APP and APLP-deficient mouse phenotypes revealed clear synaptic defects and impaired neuromuscular junction (NMJ) formation (14). The analysis of the different combinations of APP/APLP knockouts (KOs) indicated a prominent role of APP and APLP2 in NMJs (15). The APP family is thus involved in neuromuscular (NM) function and NMJ formation, but APP-specific function and the molecular mechanism associated need to be established.

We show here for the first time that the transcription of the *glial cell line-derived neurotrophic factor* (*GDNF*) gene is down-regulated in APP$^{-/-}$ mouse embryonic fibroblasts (MEFs) and in muscles of APP$^{-/-}$ mice. GDNF, initially identified as a potent survival factor for dopaminergic neurons in the CNS (16), is a trophic factor for neuronal populations of the peripheral nervous system (17). It is produced by nonneuronal cells, such as skeletal muscles, where it can act as a retrograde factor involved in NMJ formation (18–20). GDNF overexpression or GDNF injection in muscles causes multiple innervations and slows the process of synapse elimination (21, 22). We found that transcriptional regulation of *GDNF* is preferentially exerted by the APP751 isoform, highly expressed in peripheral cells. In addition, APP-dependent *GDNF* transcription appears to be independent of AICD release by γ-secretase and is not requiring the intracellular region of APP. Using a new nerve–muscle coculture system, we found that APP knockdown resulted in defective muscular differentiation and impaired formation of contacts between muscle and neuronal cells. Finally, we showed that electroporation of GDNF expression vectors in muscles of APP$^{-/-}$ mice restores the NMJ synaptic morphology, indicating that APP-dependent GDNF expression in muscles is a critical process in the establishment of NMJs.

MATERIALS AND METHODS

Chemicals and reagents

Cell culture media and reagents, Lipofectamine 2000 Reagent, NuPAGE 4–12% Bis-Tris Gels, and staining NuPAGE blue were from Invitrogen (Life Technologies, Carlsbad, CA, USA); *N*-[*N*-(3,5-difluorophenacetyl)-L-alanyl]-sphenylglycine t-butyl ester (DAPT) was from Calbiochem (Camarillo, CA, USA). phGDNF plasmid was obtained from InvivoGen (San Diego, CA, USA). Restriction enzymes *Age*I and *Xba* were from Thermo Fisher Scientific (Waltham, MA, USA). Lentivirus concentrator (Lenti-X Concentrator) was purchased from Clontech Laboratories (Mountain View, CA, USA). TRIzol Reagent, FuGene, and Complete Protease Inhibitor Cocktail were from Roche (Basel, Switzerland). The cDNA Synthesis Kit and iQ SYBR Green Supermix were from Bio-Rad (Hercules, CA, USA). The Midori Green Advance dye was purchased from Nippon Genetics Europe (Düren, Germany). The small interfering RNAs (siRNAs) were ordered from Eurofins MWG Operon (Ebersberg, Germany). Reagents for luciferase assays (Dual-Glo Luciferase Assay System), the phRG-TK construct, and ELISA kit were from Promega (Fitchburg, WI, USA). Reagents for Western blotting and the BCA Protein Assay Kit were purchased from Pierce (Rockford, IL, USA); membranes and ECL+ were from GE Healthcare (Little Chalfont, United Kingdom). L-685,458 (L685), primary antibodies anti-APP 22C11, anti-C-terminal antibody (Cter), and anti-actin, and the fluorescent nucleic acid stain DAPI were obtained from Sigma-Aldrich (St. Louis, MO, USA); anti-βIII tubulin (βIIItub), anti-vesicular acetylcholine (ACh) transporter, and anti-APLP2 were from EMD Millipore (Billerica, MA, USA); rabbit anti-synaptophysin (SYN) was from Life Technologies; and Pan-neurofilament (NF) was purchased from Covance (Princeton, NJ, USA). Secondary antibodies were obtained from Amersham Biosciences (Uppsala, Sweden). The applied dilutions for each antibody were according to the manufacturer's instructions. α-Bungarotoxin (BTX) and Alexa-labeled secondary antibodies were obtained from Life Technologies. Fluorescent mounting medium was from Dako (Agilent Technologies, Santa Clara, CA, USA).

Cell culture and nerve–muscle cocultures

MEFs were cultured in DMEM/Ham's F-12 medium supplemented with 10% serum and antibiotics. C2C12 cells were grown in DMEM supplemented with 10% fetal bovine serum (FBS) and 1% nonessential amino acids. Muscular differentiation was induced by shifting myoblasts in DMEM supplemented with 1% horse serum. The myotube fusion index was calculated as the number of myotubes (defined as having at least 3 nuclei) normalized to the total amount of cells. NG108-15 cells were grown in DMEM supplemented with 10% FBS, 2% hypoxanthine, aminopterin, and thymidine, and antibiotics. Differentiation of NG108-15 cells was induced by switching from regular medium to 1% FBS medium. For nerve–muscle cocultures, 7-d-old differentiated NG108-15 cells were plated on 2-d-old myotubes and maintained in coculture for 3 d (23). Cocultures were grown in DMEM with 1% horse serum. All cell cultures were maintained at 37°C in a humidified atmosphere (5% CO_2).

Cell treatment, plasmid, and siRNA transfection

MEFs were treated by DAPT and L685 at indicated concentrations; cells and culture media were harvested 16 h after treatments. C2C12 cells were transfected with the expression vector encoding human GDNF isoform 1 (phGDNF) 24 h after seeding. The control plasmid (mock) was generated by removal of the GDNF-coding sequence. The siRNAs specifically targeting the mouse APP transcript and mismatched controls were previously described (24). The siRNAs were transfected in C2C12 24 h after seeding with Lipofectamine 2000 Reagent, according to the manufacturer's instructions. APP silencing was monitored by Western blotting 6 d after transfection.

RNA preparation, RT-PCR, and quantitative PCR

RNAs were extracted from cells and tissues in TRIzol Reagent and reverse transcribed using an iScript cDNA Synthesis Kit

(*continued from previous page*)

BDNF, brain-derived neurotrophic factor; BTX, α-bungarotoxin; CNTF, ciliary neurotrophic factor; C-ter, C-terminal antibody; DAPT, *N*-[*N*-(3,5-difluorophenacetyl)-L-alanyl]-sphenylglycine t-butyl ester; EDL, extensor digitorum longus; FBS, fetal bovine serum; GDNF, glial cell line-derived neurotrophic factor; GFRα1, glial cell line-derived neurotrophic factor family receptor subtype 1; KO, knockout; L685, L-685,458; MEF, mouse embryonic fibroblast; NF, neurofilament; NGF, nerve growth factor; NM, neuromuscular; NMJ, neuromuscular junction; qPCR, quantitative PCR; siRNA, small interfering RNA; SYN, synaptophysin; TA, tibialis anterior

(Bio-Rad). Real-time quantitative PCR (qPCR) analysis was performed on 2 ng cDNA template by using iQ SYBR Green Supermix in an iCycler IQ Multicolor Real-Time PCR Detection System (Bio-Rad). qPCR conditions were typically 95°C for 30 s, followed by 40 cycles of 30 s at 95°C, 45 s at 60°C, and 15 s at 79°C and ended by 71 cycles of 30 s at 60°C. The relative changes in the target gene:glyceraldehyde 3-phosphate dehydrogenase mRNA ratio were determined by the $2^{(-\Delta\Delta Ct)}$ calculation. The sequences for qPCR primers are the following: GDNF, forward 5′-TTAATGTCCAACTGGGGGTCT-3′ and reverse 5′-GCCGAGGGAGTGGTCTTC-3′; human GDNF, forward 5′-CCAACCCAGAGAATTCCAGA-3′ and reverse 5′-AGCCGCTGCAGTACCTAAAA-3′; brain-derived neurotrophic factor (BDNF), forward 5′-GCGGACCCATGGGACTCT-3′ and reverse 5′-AGCCAGTGATGTCGTCGTC-3′; nerve growth factor (NGF), forward 5′-TGATCGGCGTACAGGCAGA-3′ and reverse 5′-GAGGGCTGTGTCAAGGGAA-3′; ciliary neurotrophic factor (CNTF), forward 5′-TGGCTTTCGCAGAGCAATCAC-3′ and reverse 5′-GCAGTCAGGTCTGAACGAATCTT-3′; IGF-1, forward 5′-TCATGTCGTCTTCACACCTCTTCT-3′ and reverse 5′-CACACACGAACTGAAGAGCAT-3′; IGF-2, forward 5′-ACAACTTCGATTTGAACCACATTC-3′ and reverse 5′-GAGAGCTCAAACCATGCAAACT-3′; and glyceraldehyde 3-phosphate dehydrogenase, forward 5′-ACCCAGAAGACTGTGGATGG-3′ and reverse 5′-ACACATTGGGGGTAGGAACA-3′.

Reporter gene assays

MEF cells were transfected with pGL3-Luc, pGL3-GDNF-Luc, and phRG-TK (0.2 μg per well) mixed to FuGene Reagent according to the manufacturer's instructions. Cells were rinsed 48 h after transfection with PBS and incubated with the reporter lysis buffer (Promega) for 15 min at room temperature. Firefly and *Renilla* luciferase activities were measured with the Dual-Glo Luciferase Assay System on a Sirius Luminometer (Berthold, Pforzheim, Germany). Firefly luciferase activity was standardized by the *Renilla* luciferase activity to correct for transfection efficiency.

ELISA

Secreted GDNF levels were quantified in cell media by ELISA following the manufacturer's instructions (Promega). A sample of culture medium was collected on ice, quickly centrifuged to remove cell debris, and kept at −20°C after adding a Complete Protease Inhibitor Cocktail.

Lentivirus-mediated APP stable expression

MEFs stably expressing human APP695, human APP751, and human APP751 truncated in its C-terminal region from residue 709 to residue 751 (APP751ΔC) in an $APP^{-/-}$ background were generated by subcloning the respective APP cDNA sequences in the *Xba*I restriction sites of a lentiviral backbone vector (plentiCMV/TOpuro) and in the *Age*I and *Xba*I restriction sites of a lentiviral backbone vector (pTM898neo). Lentiviruses were produced by cotransfection of the lentiviral packaging (gag-pol, rev, and VsVg) into human embryonic kidney 293T cells (human embryonic kidney-293 cells expressing the large T-antigen of simian virus 40). Supernatants containing the lentiviruses were harvested 48 h after transfection. The lentiviruses were concentrated and purified with the Lenti-X Concentrator kit according to the manufacturer's instructions. MEF $APP^{-/-}$ cells were transduced by the lentiviral particles followed by puromycin selection for 10 d. Stable APP expression in selected cell lines was evaluated by Western blotting.

Western blotting

Cells were rinsed and scraped off in PBS and centrifuged for 5 min at 10,000 rpm. Pellets were sonicated in lysis buffer [125 mM Tris (pH 6.8), 20% glycerol, and 4% sodium dodecyl sulfate] with Complete Protease Inhibitor Cocktail. Protein concentration was determined by the BCA Protein Assay Kit. A total of 15 μg protein was heated for 10 min at 70°C in loading buffer (lysis buffer containing 0.5 M DTT and staining NuPAGE blue), loaded and separated onto NuPAGE 4–12% Bis-Tris Gel, and then transferred for 2 h at 30 V onto nitrocellulose membranes. After blocking (5% nonfat milk in PBS), membranes were incubated overnight at 4°C with the primary antibodies, washed, and incubated with the secondary antibodies coupled to peroxidase prior to ECL detection (GE Healthcare). ECL signals were quantified with a Gel Doc 2000 Imaging System coupled to Quantity One software (Bio-Rad). Primary antibodies included anti-APP 22C11 (1:500), anti-APLP2 (1:2000), anti-Cter (1:2000), anti-βIIItub (1:1000), anti-SYN (1:2000), or with anti-actin antibody (1:3000). Secondary antibodies included anti-mouse (1:10,000) or anti-rabbit (1:10,000).

Immunocytochemistry

Acetylcholine receptors (AChRs) were blocked with BTX-Alexa 594 (1:2000) by adding the blocker in the medium for 40 min at 37°C at the end of the coculture. Following incubation, cells were rinsed twice with PBS and fixed with 4% paraformaldehyde for 15 min. After 3 washes in PBS, cells were permeabilized with 1× PBS/0.3% Triton X-100 for 30 min and saturated with 1× PBS/5% goat serum/0.1% Triton X-100 for 30 min. Primary antibodies were prepared in the blocking solution and incubated overnight at 4°C with gentle shaking. Primary antibodies used were mouse anti-βIIItub (1:6000) and the rabbit anti-SYN (1:250). After 3 washes in PBS, cells were incubated with secondary antibodies (goat anti-mouse Alexa 488 and goat anti-rabbit Alexa 647; 1:500 in blocking solution). DAPI was incubated with secondary antibodies for 1 h at 4°C with gentle shaking. After 3 washes in PBS, cocultures were stored with 0.1% PBS-azide at 4°C. Pictures were acquired with an Evos fluorescence microscope (Advanced Microscopy Group, Mill Creek, WA, USA). Imaging analyses were performed with ImageJ software (National Institutes of Health, Bethesda, MD, USA).

Animal models

The $APP^{+/+}$ and $APP^{-/-}$ mice were obtained from The Jackson Laboratory (Bar Harbor, ME, USA) as C57Bl/6J and backcrossed for >5 generations to the CD1 genetic background. Only male mice were used for experiments. Animal care and handling were performed according to the Declaration of Helsinki and approved by the Animal Ethics Committee of the Université Catholique of Louvain.

Muscle histology

Tibialis anterior (TA) muscle transversal section area was measured from 200 fibers using a homemade planimetry program as previously described (25). Briefly, paraffin-embedded TA muscles were deparaffinated, rehydrated and stained with hematoxylin/eosin, and mounted with Entellan (Merck, EMD Millipore).

Mechanical measurement

The isometric force of muscles from 3- and 8-wk-old $APP^{+/+}$ and $APP^{-/-}$ mice was recorded as previously described (26). Mice

were deeply anesthetized by intraperitoneal injection of a solution containing ketamine (10 mg/ml) and xylazine (1 mg/ml) in order to preserve muscle perfusion during dissection of the extensor digitorum longus (EDL) muscle. EDL muscle was bathed in a 1 ml horizontal chamber continuously superfused with 4-(2-hydroxyethyl)-1-piperazineethanesulfonic acid-buffered Krebs solution (100% O_2) containing 135.5 mM NaCl, 5.9 mM KCl, 1.2 mM $MgCl_2$, 2.5 mM $CaCl_2$, 11.6 mM 4-(2-hydroxyethyl)-1-piperazineethanesulfonic acid sodium and 11.5 mM glucose and maintained at a temperature of 20 ± 0.1°C. One end of the muscle was tied to an isometric force transducer and the other to an electromagnetic motor and length transducer. Stimulation (125 Hz) was delivered through platinum electrodes running in parallel to the muscles. Optimum muscle length was carefully adjusted for maximal isometric force using 300 ms maximally fused tetani. Force was digitalized at a sampling rate of 1 kHz, using a PCI 6023E i/o card (under a homemade LabView program; National Instruments, Austin, TX, USA). Normalized stress was expressed relative to cross-sectional area, obtained by multiplying absolute force by the ratio muscle fiber length (millimeter):muscle blotted weight (milligram) and considering the fiber length equal to 0.5 × L0, where *L0* is optimum muscle length.

Immunohistochemistry

Mice were anesthetized with ketamine (75 mg/kg Ketalar; Pfizer, Brussels, Belgium) and xylazine (5 mg/kg Rompun; Bayer Healthcare, Diegem, Belgium) solution and perfused transcardially with 4% paraformaldehyde in PBS. Limb muscles were dissected and prepared for immunohistochemistry as previously described (27). Briefly, muscle cryosections were treated with 0.1 M glycine in PBS for 30 min; after 3 washes in PBS, sections were permeabilized with 1× PBS/0.3% Triton X-100 for 10 min and saturated with 1× PBS/0.3% Triton X-100/10% bovine serum albumin for 45 min. Primary antibodies were prepared in the blocking solution and incubated overnight at 4°C with gentle shaking. After 3 washes in PBS, cells were incubated with secondary antibodies (goat anti-mouse Alexa 488 and goat anti-rabbit Alexa 647; 1:500 in blocking solution). DAPI was incubated with secondary antibodies for 1 h at 4°C with gentle shaking. After 3 washes in PBS, cocultures were stored with 0.1% PBS-azide at 4°C. Primary antibodies for immunofluorescence were the mouse anti-Pan-NF (1:2000) and rabbit anti-SYN (1:250). Secondary antibodies (1:2000) were anti-mouse Alexa Fluor 488 and anti-rabbit Alexa Fluor 647. BTX-Alexa 594 (1:2000) was incubated with the secondary antibodies. Pictures were taken with an Olympus FluoView confocal microscope (Olympus America Inc., Center Valley, PA, USA).

Plasmid injection and electroporation

Injection and electroporation procedures have been previously described (28). Briefly, mice were intraperitoneally injected with an anesthetic solution of ketamine and xylazine. A total of 5 μg phGDNF or mock plasmid diluted in 20 μl PBS was injected into each tibial cranial muscle by using an insulin syringe. Plasmids were prepared using the EndoFree Plasmid Mega Kit (QIAGEN, Venlo, The Netherlands). Plasmids were diluted in PBS and stored at −20°C. Immediately after injection, the leg was placed between 3-mm–spaced plate electrodes (BTX Caliper Electrodes), and 8 square-wave electric pulses (200 V/cm 20 ms 2 Hz) were delivered by a Gemini System generator (BTX; both from VWR International, Leuven, Belgium). A conductive gel was used to ensure electrical contact with the skin (Aquasonic 100; Parker Laboratories, Inc., Fairfield, NJ, USA).

Statistical analysis

The number of samples in each experimental condition is indicated in the figure legends. Data were analyzed using GraphPad Prism software (GraphPad Software, La Jolla, CA, USA) by ANOVA followed by unpaired Student's *t* test (2 experimental conditions) or by Tukey's and Bonferroni's multiple comparison tests (>2 experimental conditions).

RESULTS

APP-dependent *GDNF* transcription in fibroblasts and muscles

We identified in a transcriptome analysis (MEF APP $^{+/+}$ *vs.* $^{-/-}$) a set of genes (Supplemental Fig. S1), including *GDNF*, that were transcriptionally regulated by APP and met stringent criteria fold change (>3 or <3; difference between mean intensity >100). Quantitative RT-PCR confirmed a strong decrease (80%) in GDNF mRNA levels measured in $APP^{-/-}$ MEFs when compared to $APP^{+/+}$ (**Fig. 1*A***). The mRNA levels of other neuronal (BDNF, NGF, and CNTF) and nonneuronal growth factors (IGF-1 and IGF-2) were not affected by the absence of APP in MEF cells (Fig. 1*A*). Consistently, secreted GDNF levels were also decreased in $APP^{-/-}$ MEFs (Fig. 1*B*). Experiments carried out with a luciferase reporter gene (pGL3-GDNF-Luc) harboring a 1.5 kb fragment of the *GDNF* promoter (17) evidenced that the transcriptional activity of the *GDNF* promoter was strongly reduced (~70–80%) in $APP^{-/-}$ cells when compared to $APP^{+/+}$ (Fig. 1*C*). To further confirm that APP specifically regulates GDNF expression, rescue experiments were performed in $APP^{-/-}$ MEFs stably expressing 1 of the 2 major isoforms of human APP: APP695 and APP751 (695r and 751r) (Fig. 1*D*). APP-dependent regulation of GDNF expression appeared to be isoform specific. GDNF expression was significantly restored by stable re-expression of APP751 in $APP^{-/-}$ cells, but not by APP695 (the neuronal isoform) (Fig. 1*E*, *F*).

MEFs were treated with the specific γ-secretase inhibitors DAPT and L685 at the concentration of 10 μM for 16 h, to block AICD release. We observed the accumulation of C-terminal fragments in the treated cells, which is the hallmark of the inhibition of γ-cleavage (**Fig. 2*A***). Treatment by γ-secretase inhibitors did not increase the production of other APP metabolites, including soluble APPα (data not shown). In these conditions, we did not observe a significant effect on GDNF mRNA levels (Fig. 2*B*). Moreover, rescue experiments were performed in $APP^{-/-}$ MEFs by stably expressing APP751 deleted of its C-terminal domain (APP751ΔCr) (Fig. 2*C*). GDNF expression appeared to be significantly restored by APP751ΔCr, indicating that the APP C-terminal domain is not involved in the regulation of GDNF expression (Fig. 2*D*).

We measured GDNF mRNA expression in the *quadriceps* of young and adult mice, and we observed that GDNF mRNA levels were significantly lower in $APP^{-/-}$ muscles (**Fig. 3**). Interestingly, the other neuronal and nonneuronal growth factors previously tested in MEF cells (BDNF, NGF, CNTF, IGF-1, and IGF-2) were not differentially expressed in muscles in the absence of APP, demonstrating that APP specifically regulates GDNF expression also in muscles (Fig. 3).

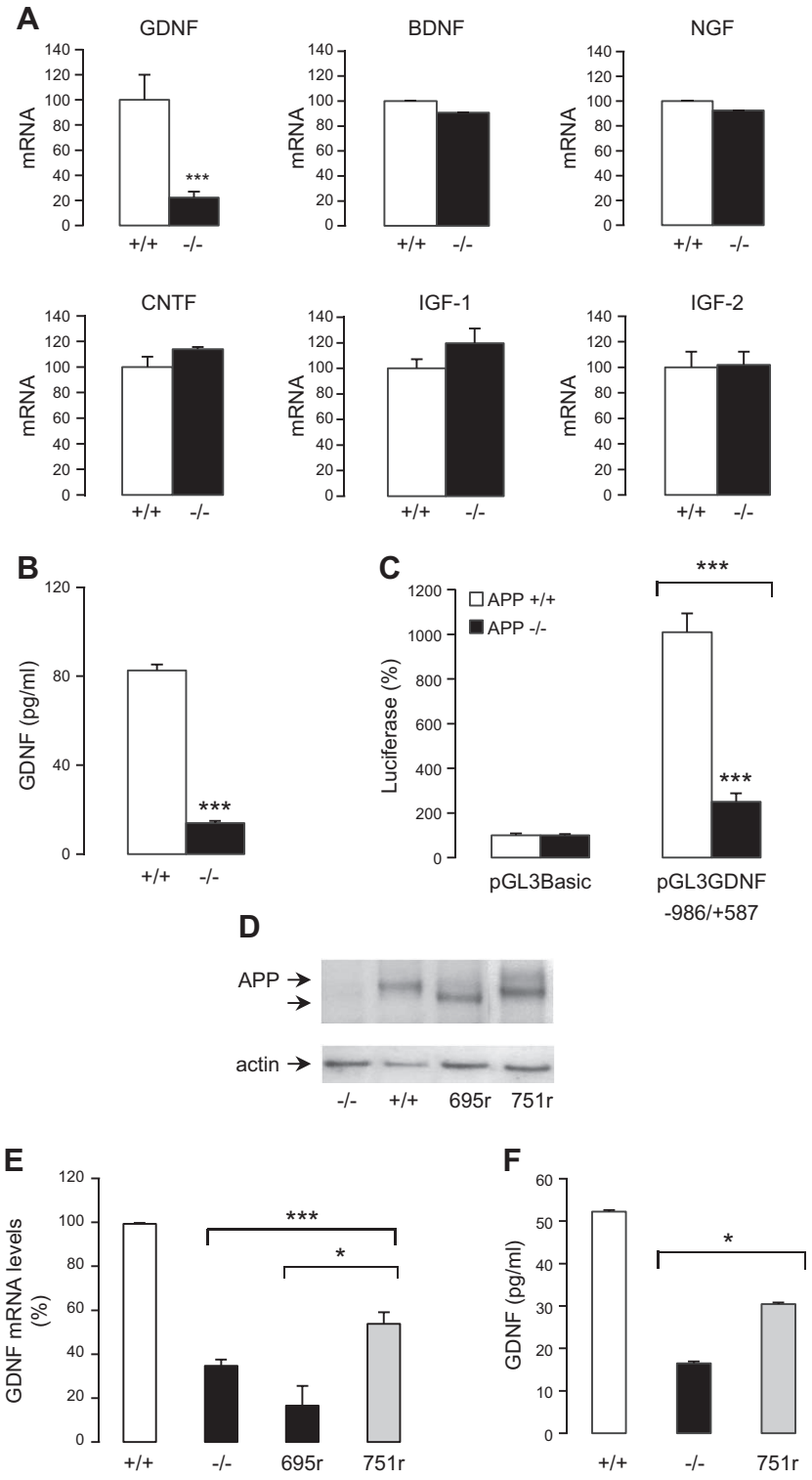

Figure 1. APP controls GDNF transcription and expression in fibroblasts in an APP751 isoform-dependent way. Experiments were carried out in APP-null ($APP^{-/-}$) MEF cells and respective controls ($APP^{+/+}$). *A*) Comparative qPCR analysis of GDNF, BDNF, NGF, CNTF, IGF-1, and IGF-2 mRNA levels. Results (means ± SEM) are expressed as the percentage of mRNA levels measured in $APP^{+/+}$. ***$P < 0.001$, Student's t test (n = 4). *B*) GDNF-secreted levels (picograms per milliliter) were quantified by ELISA. Values (means ± SEM) are given in picograms per milliliter. ***$P < 0.001$, Student's t test ($n = 4$). *C*) GDNF promoter transcriptional activity (luciferase) in $APP^{+/+}$ or $APP^{-/-}$ MEFs transfected with either the pGL3-BASIC or the pGL3-GDNF-Luc constructs, measured 48 h after transfection. Results (means ± SEM) are expressed as the percentage of pGL3 basal activity. ***$P < 0.001$, compared to control (pGL3-BASIC) or as indicated, Bonferroni's multiple comparison test ($n = 4$). Rescued MEF cell lines expressed levels of APP695 or 751 similar to those detected in $APP^{+/+}$ MEFs. Cell lysates were analyzed by Western blotting, revealed with the anti-APP 22C11 antibody. Actin was used as a protein loading control (*D*). *E*) qPCR analysis of GDNF mRNA in $APP^{+/+}$, $APP^{-/-}$, 695r, and 751r. Results (means ± SEM) are expressed as the percentage of GDNF mRNA levels measured in $APP^{+/+}$. ***$P < 0.001$ and *$P < 0.05$, compared to $APP^{+/+}$ or as indicated, Bonferroni's multiple comparison test ($n = 9$ at least). The analysis of GDNF mRNA levels (*E*) and protein levels (F) in these cells showed that APP751, but not APP695, partially restored GDNF expression.

Impaired force production and muscle atrophy in $APP^{-/-}$ mice

$APP^{-/-}$ mice show mainly an NM phenotype. Our experiments confirmed that $APP^{-/-}$ mice show reduced grip strength compared to control mice (Supplemental Fig. S2). The muscle functionality was evaluated by mechanical experiments. Isolated EDL muscles were maximally stimulated to obtain fused tetani. Muscles from $APP^{-/-}$ mice developed a reduced maximal tetanic stress at 3 wk of age and even more importantly at 2 mo of age (**Fig. 4*A***), without any significant shift in the sensitivity to the frequency of stimulation (unpublished results), indicating that the muscles did not obviously change their fast phenotype to a slow one. Deficiency in force production of $APP^{-/-}$ mice could then result from a morphologic defect in skeletal muscle development. We characterized histologically muscles from $APP^{+/+}$ and $APP^{-/-}$ mice. TA muscles were

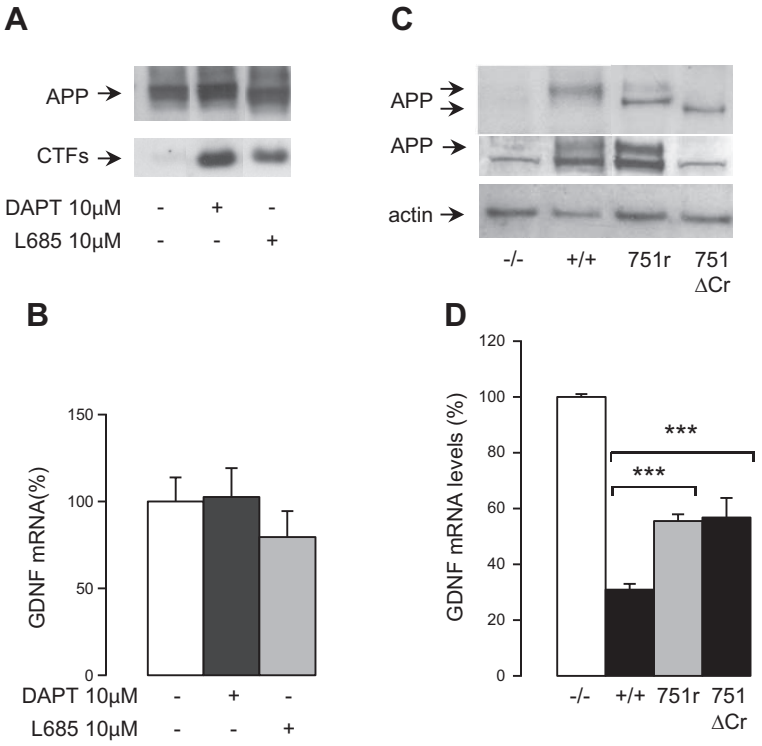

Figure 2. AICD is not involved in GDNF regulation. *A*) MEF APP$^{+/+}$ cells were treated for 16 h with 10 μM DAPT and L685. Western blotting was revealed with the anti-Cter. *B*) GDNF mRNA levels. Results (means ± SEM) are expressed as the percentage of mRNA levels measured in APP$^{+/+}$ nontreated cells. *C*) Rescued MEFs expressed levels of APP751 or 751ΔCr comparable to those detected in APP$^{+/+}$ MEFs as observed by Western blotting on cell lysates revealed with the anti-APP 22C11 antibody. Western blotting revealed with the anti-Cter confirmed the absence of signal for the $^{-/-}$ and for the ΔC construction. Actin was used as a protein loading control (*C*). These images have been spliced for clarity. Original captures are included in Supplemental Data (*A*, *C*). *D*) qPCR analysis of GDNF mRNA in APP$^{+/+}$, APP$^{-/-}$, 751r, and 751ΔCr. Results (means ± SEM) are expressed as the percentage of GDNF mRNA levels measured in APP$^{+/+}$. ***$P < 0.001$ compared to APP$^{+/+}$, Bonferroni's multiple comparison test ($n = 3$).

collected and stained with hematoxylin/eosin (Fig. 4*B*). Cross-sectional area measured in >200 fibers of TA muscles from 6 different animals (Fig. 4*C*) revealed an important decrease in the mean fiber size from APP$^{-/-}$ mice compared to control littermates at 2 mo of age (1198 ± 49 μm^2 *versus* 1952 ± 187 μm^2). The distribution patterns of cross-sectional areas of fibers clearly showed a shift of the curve of cross-sectional area to smaller values in APP$^{-/-}$ muscles at 2 mo of age (Fig. 4*D*).

Altered distribution and decreased ACh vesicle density in NMJs of APP$^{-/-}$ mice

The functional and morphologic phenotype we observed in muscles from APP$^{-/-}$ mice could result from an altered neuronal innervation or defects in muscle cell differentiation *per se*. We analyzed connections between motor nerve terminals and muscles, the NMJs, at birth, 3 wk, and 2 mo of age in order to assess whether the muscular phenotype can be related to defective formation or abnormal stabilization and maintenance of NMJs in the absence of APP. At birth, the AChRs were arranged in plaques overlaid to sparse dotted SYN aggregates corresponding to presynaptic vesicles, indicating that the motor nerve terminals began to be affixed to the motor end plates both in wild-type and KO mice. The initiation of NMJ formation takes, indeed, place normally even in the absence of APP (Supplemental Fig. S3). At 3 wk, when the development and maturation of NMJs are completed, APP$^{+/+}$ displayed a "pretzel-like" shape typical of an expected single innervated junction with an intense SYN labeling (**Fig. 5*Aa–c′***). At the same age,

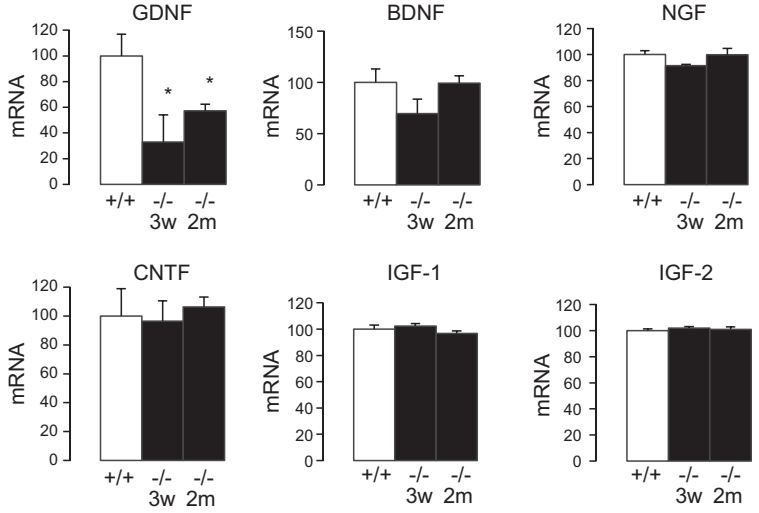

Figure 3. APP controls *GDNF* transcription and expression in the *quadriceps ex vivo*. qPCR analysis of GDNF mRNA expression in the *quadriceps* from 3-wk-old (3w) and 2-mo-old (2m) APP$^{+/+}$ and APP$^{-/-}$ mice is shown. BDNF, NGF, CNTF, IGF-1, and IGF-2 mRNA levels have been monitored in the same experiments. Results (means ± SEM) are expressed as the percentage of mRNA levels measured in APP$^{+/+}$. *$P < 0.05$, Bonferroni's multiple comparison test ($n = 4$).

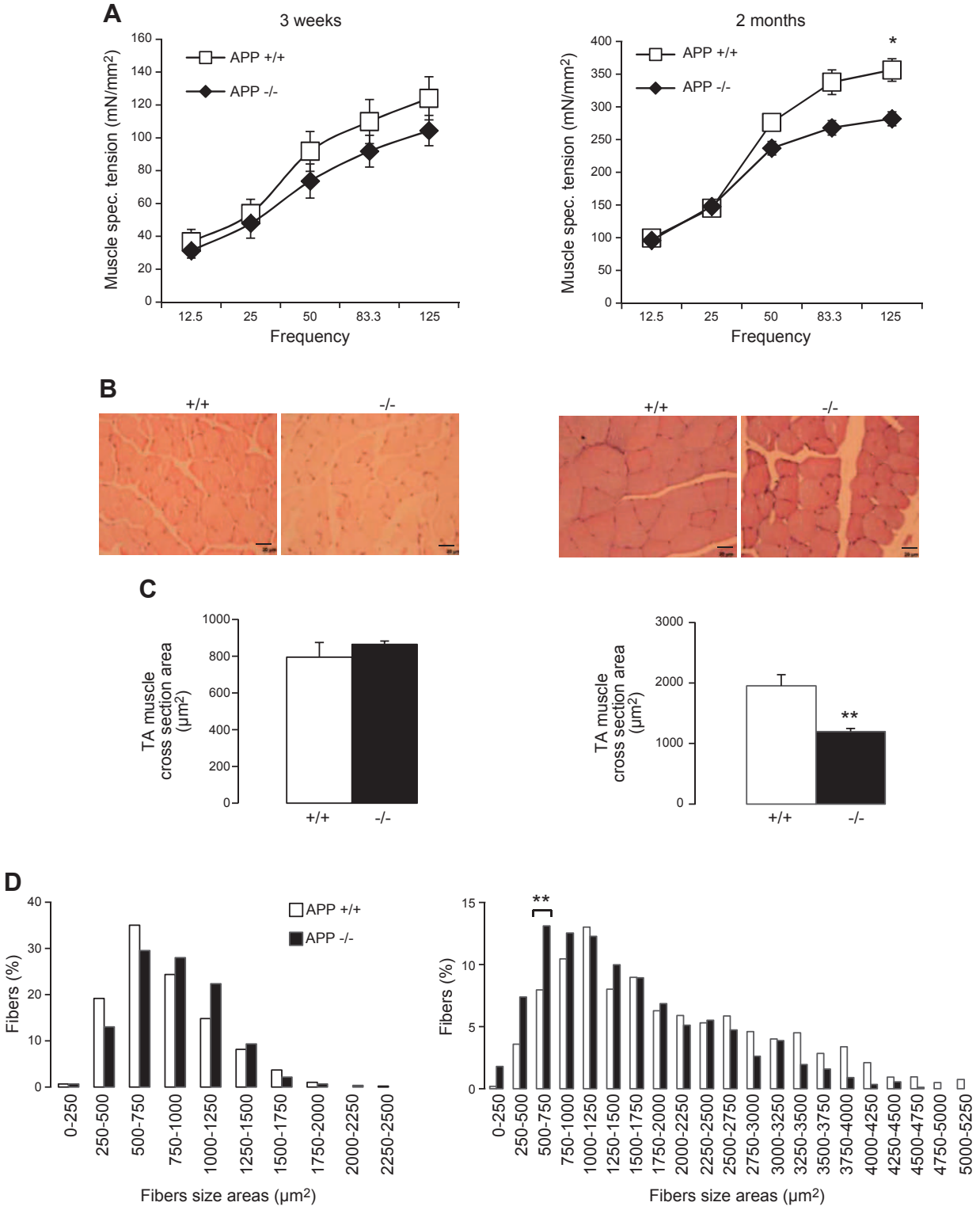

Figure 4. APP$^{-/-}$ mice show impaired muscular strength and muscular atrophy *ex vivo*. *A*) Muscle-specific (spec.) tension expressed in millinewtons per squared millimeter (mN/mm^2) in function of stimulation frequency. *$P < 0.05$, Tukey's test (n = 5 mice). *B*) Muscle cross section from 3-wk- and 2-mo-old APP$^{+/+}$ and APP$^{-/-}$ mice after hematoxylin/eosin staining of TA muscles. *C*) TA muscle fiber cross section area at 3 wk or 2 mo of age. Values (means ± SEM) are muscle cross section areas. **$P < 0.01$, Student's t test (n = 6 mice; 200 muscle fibers counted per muscle), compared to APP$^{+/+}$ (cross section areas). *D*) Quantification of fiber subpopulations by area size at 3 wk or 2 mo of age. Values (means ± SEM) are fiber size distribution as the percentage of total number of fibers counted in 1 cross section. **$P < 0.01$, χ^2, Pearson's test (n = 6 mice), compared to APP$^{+/+}$ (fiber size distribution).

an important decrease in SYN labeling was observed at motor nerve terminals in APP$^{-/-}$ mice (Fig. 5*AA–C′*). At 2 mo, junctions still displayed a pretzel-like shape with an intense SYN labeling in APP$^{+/+}$ mice (Fig. 5*Ad–f′*). The morphology of the motor end plate in APP$^{-/-}$ mice showed that some of them were innervated, but the SYN staining was much weaker, if detectable (Fig. 5*AD, D′*). Other junctions were not innervated by the motor nerve terminal, and consequently, SYN labeling was faint or absent (Fig. 5*AE–F′*). Thus, in the absence of APP, ACh vesicles do not properly localize at the motor nerve terminals, and their density is significantly reduced. This was confirmed by the quantification of SYN (Fig. 5*B*). Area measurements indicated that NMJ dimensions are not affected by lack of APP (Fig. 5*C*).

APP-dependent GDNF expression in muscle cells drives the formation of NM contacts *in vitro*

We used *in vitro* muscle cell cultures or neuronal/muscle cell coculture to gain insight into the role of APP-dependent GDNF expression in NMJ formation. Levels of secreted GDNF increased significantly upon differentiation of C2C12 muscle cells (**Fig. 6*A***) as well as APP levels (Fig. 6*B*). Moreover, increasing GDNF expression by transfection of an expression vector triggered muscle cell differentiation and fusion (Fig. 6*C–E*). The effect of acute APP knockdown on myoblast fusion in C2C12 cells was analyzed by siRNAs specifically targeting mouse APP (si7 and si8) compared to mismatched controls (M7 and M8). Both si7 and si8 reduced by 50% APP expression (Fig. 6*D*). We selected si8 for further experiments because the M7 mismatched control also decreased APP levels as opposed to M8. These siRNAs (si8) did not induce toxicity or off-target effects, as verified by the identical levels of APLP2 expression upon si8 transfection (Fig. 6*D*). Myotube formation was reduced by 50% after 3 d of differentiation in APP-silenced cells, and GDNF expression upon APP silencing significantly restored it (Fig. 6*G*). Thus, increased APP levels are directly related to C1C12 muscle cell differentiation, and this process is parallel to an increase in GDNF secretion.

We next set up a new *in vitro* model of nerve–muscle cocultures in which C2C12 cells were cultured and transfected with APP siRNAs prior to transfection or not with a GDNF-expressing vector. Myoblast differentiation was induced 8 h after transfection and 2 d after differentiated cholinergic NG108-15 neuronal cells were added on myotubes, and NM contact formation was studied after 3 d of coculture. In coculture with differentiated C2C12 cells, cholinergic NG108-15 neuronal cells extend neurites to make connections with myotubes after 72 h (**Fig. 7**). APP silencing (si8) in muscle cells remains very efficient after adding the differentiated NG108-15 cells (Fig. 7*A*). GDNF secretion was significantly reduced by ±20% under these conditions (Fig. 7*B*). A similar decrease in GDNF-secreted levels (±25%) was still observed in APP-silenced cultures transfected by a GDNF expression plasmid (Fig. 7*C*), likely due to the decrease in endogenous GDNF production induced by APP silencing. This coculture model allowed us to analyze the NM contacts by staining both the presynaptic compartment with NF (Fig. 7*Da*) and ACh vesicle (SYN, Fig. 7*Db*) markers and the postsynaptic clusters of AChRs with BTX (Fig. 7*Dc*). The establishment of NM contact is defined by the colocalization of the 3 markers (Fig. 7*Dd*). We observed a significant decrease of 35% in the number of contacts upon APP silencing (Fig. 7*E*). When GDNF expression was rescued in muscle cells, the defect was specifically recovered only in APP-silenced cocultures (si8) (Fig. 7*F*). Importantly, the positive effects of exogenous GDNF expression were significant in cocultures where APP was previously silenced, but not in control conditions, meaning that the effect is not resulting from simple GDNF overexpression (Fig. 7*G*).

APP-dependent GDNF expression affects synaptic vesicle formation and neuronal morphology *in vitro*

The *in vitro* cocultures enabled us to study the impact of APP down-regulation and subsequent GDNF decrease on the morphology of neuronal cells. The intensity of presynaptic vesicle labeling was reduced in cocultures after APP silencing in muscle cells (**Fig. 8*A***). This pattern was comparable to the one observed at the motor end plate *in vivo* (see Fig. 5). SYN levels (Fig. 8*B*) confirmed a reduction of ACh vesicles when compared to controls. The localization and density of ACh vesicles at neuronal active zones, rather than neuronal abundance, were impaired by APP silencing in muscle cells (Fig. 8*C*, left panels) and restored by GDNF expression (Fig. 8*C*, right panels).

We next studied neuronal maturation by measuring the length of neuronal outgrowths and analyzing the dendritic arborization by counting the neuronal branches. An example of a mature cholinergic neuron with a tertiary specialization is shown in Fig. 8*D*. The quantitative analysis of neuronal maturation in the different coculture conditions is illustrated in **Table 1**. Axons from APP-silenced cocultures were 25% shorter when compared to control conditions and never showed tertiary arborizations (Fig. 8*C*; quantification in Table 1). Exogenous GDNF expression induced an important morphologic recovery of axonal length and neuronal branching in APP-silenced cocultures (Fig. 8*C*; quantification in Table 1).

In vivo GDNF electroporation restores proper NMJ formation in APP$^{-/-}$ mice

We finally investigated the effects of muscular GDNF expression on NMJ formation *in vivo*. Three-week-old APP$^{+/+}$ and APP$^{-/-}$ mice were treated by electroporation with 5 μg phGDNF in the tibialis. Mice electroporated with the empty vector (mock) were used as a control. *In vivo* electroporation is the most efficient nonviral strategy of gene delivery, and skeletal muscle is the most widely targeted tissue. In particular, it is reported that green fluorescent protein expression in electroporated tibialis muscle reaches up to 90% (29). This method leads to optimal expression and spatial distribution of the transgene (30). At 10 d after electroporation, we measured the grip strength, and then mice were sacrificed for immunohistochemistry analysis. We observed by qPCR on the tibialis high expression of phGDNF mRNA and only in the GDNF-electroporated mice (**Fig. 9*A***). No significant differences have been observed in the grip strength of mice before and

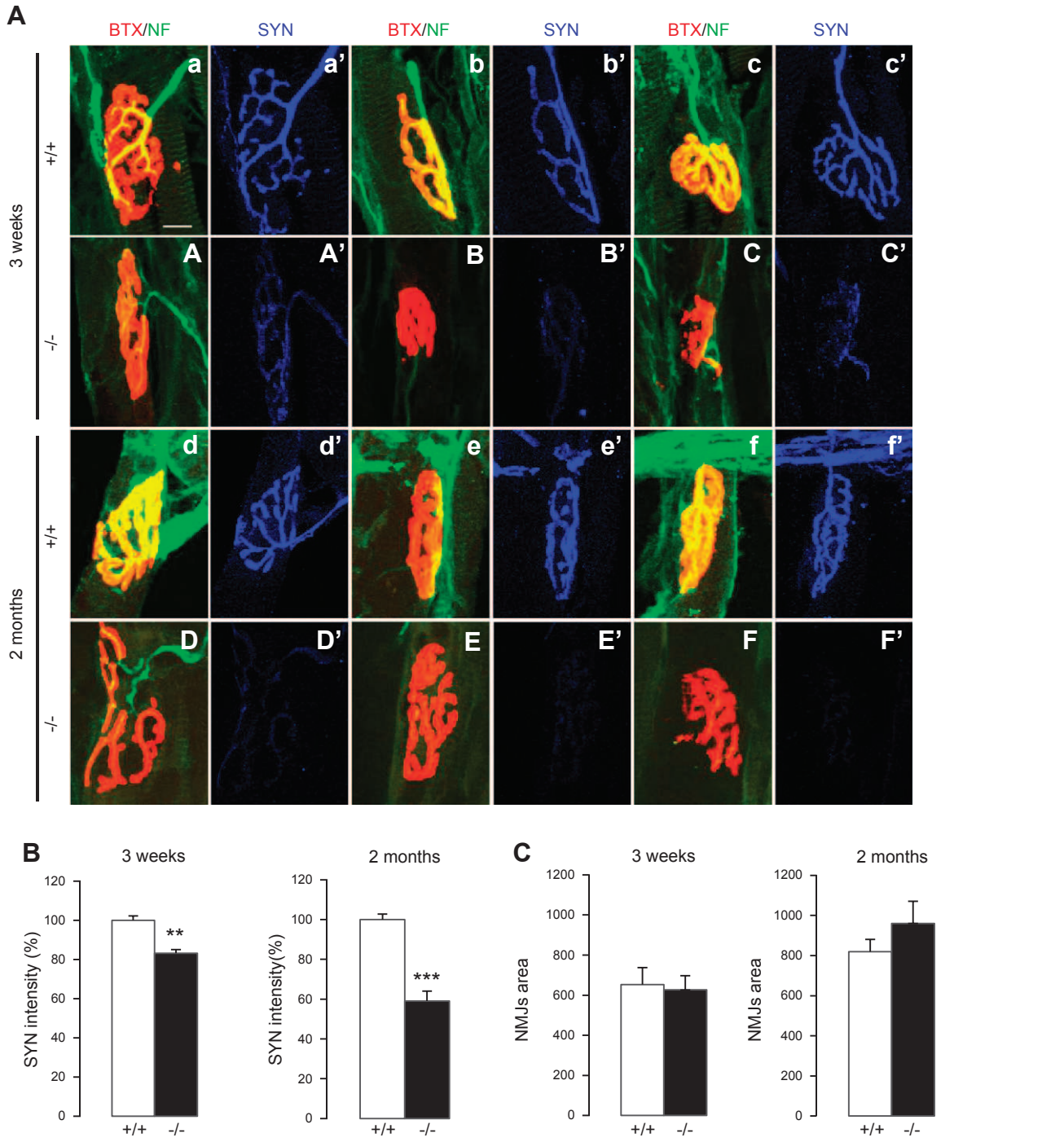

Figure 5. Absence of APP leads to defective motor end plate maturation and reduction of SYN intensity. Experiments were done on hindlimb sections of $APP^{+/+}$ or $APP^{-/-}$ mice at 3 wk or 2 mo of age. Stainings of pre- and postsynaptic compartments have been analyzed by confocal microscopy to generate z-stack images. *A*) Labeling of AChRs with BTX in red, immunofluorescence detection of NF in green, and of SYN in blue. Typical images are shown for 3-wk-old (*a–c′* and *A–C′*) and 2-mo-old (*d–f′* and *D–F′*) mice. Scale bar, 5 μm. *B*) Quantification of SYN intensity from z-stack images of at least 20 NMJs per animal ($n = 3$) at 3 wk or 2 mo of age. Values are given as the percentage of staining intensity measured in $APP^{+/+}$ controls. $^{**}P < 0.01$ and $^{***}P < 0.001$, Student's *t* test ($n = 3$). *C*) Quantification of NMJ area (squared micrometer) in the same conditions as (*B*).

after the treatment (data not shown), although a trend toward increased grip strength appeared in electroporated mice. Importantly, muscular delivery of GDNF was able to restore ACh vesicle density at the NMJs of phGDNF-electroporated $APP^{-/-}$ mice (Fig. 9*B*), correcting the aberrant synaptic morphology induced by APP deficiency.

DISCUSSION

We demonstrated that APP controls *GDNF* transcription in MEFs and muscles. This appears to be specific to GDNF because the expression of other neurotrophins or growth factors like BDNF, NGF, CNTF, and IGF-1 and -2 is indeed

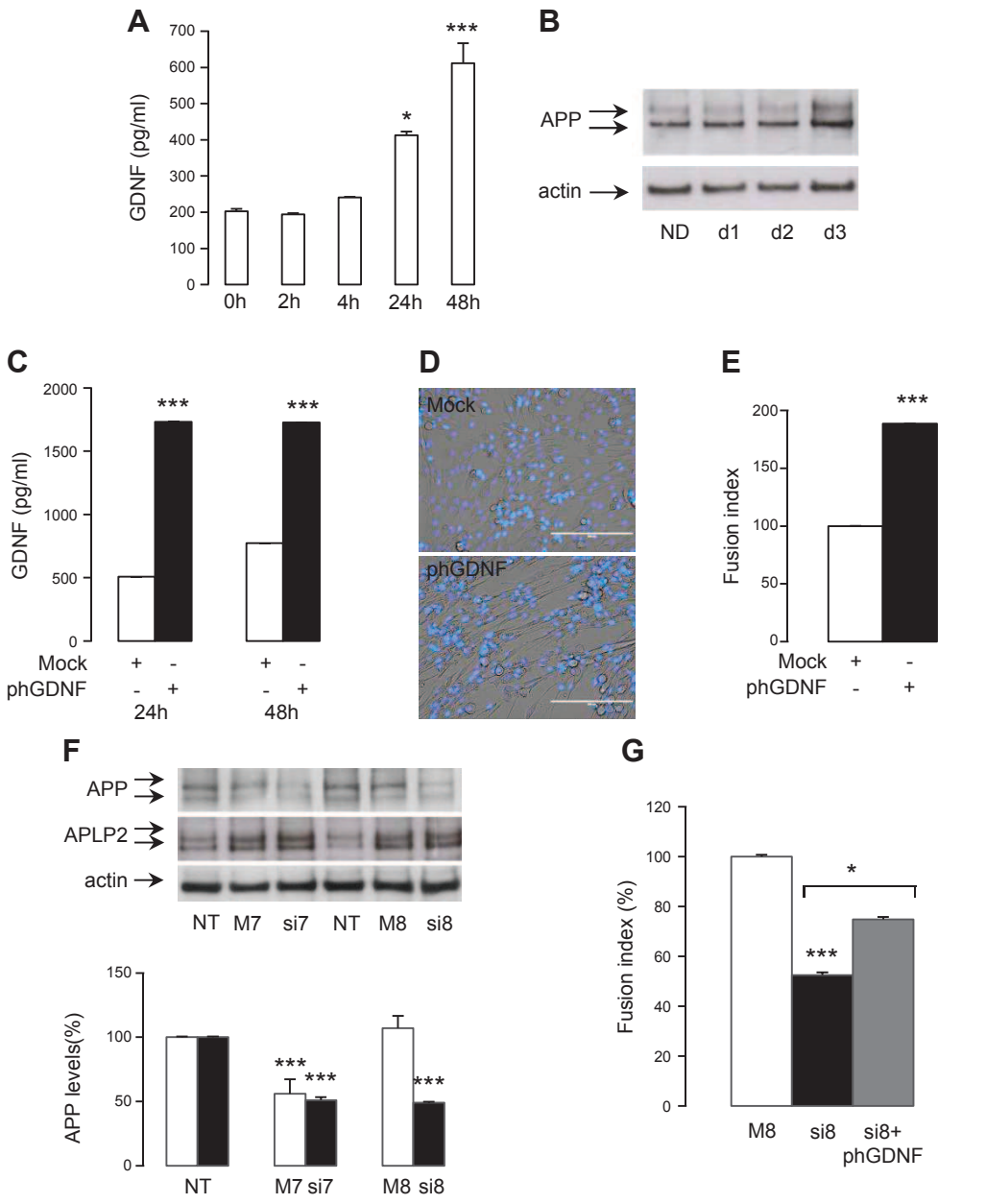

Figure 6. GDNF and APP drive the process of muscular differentiation. *A*) Secreted GDNF levels (picograms per milliliter) were measured by ELISA at indicated times after shifting C2C12 cells to differentiation medium. *B*) APP levels were analyzed by Western blotting of nondifferentiated C2C12 cell lysates (ND) or after 2, 4, or 3 d of differentiation (d1, d2, and d3). Actin was used as a loading control probe. *C*) GDNF release measured by ELISA in phGDNF-transfected C2C12. Values (means ± SEM) are given in picograms per milliliter measured in culture medium at indicated times. ***$P < 0.001$, Student's *t* test ($n = 4$). *D*) Morphology of C2C12 cells transfected with phGDNF after 3 d of differentiation. Scale bars, 200 μm. *E*) Quantification of fusion index. Values (means ± SEM) are given as the percentage of the fusion index measured in mock-transfected cells. ***$P < 0.001$, Student's *t* test ($n = 4$). *F*) The efficiency of different siRNAs (si7 and si8) directed against APP and APLP2 and their mismatched controls (M7 and M8) was tested by Western blotting of C2C12 cell lysates. Quantifications (means ± SEM) are given as the percentage of APP levels measured in nontransfected (NT) control cells. ***$P < 0.001$, Bonferroni's multiple comparison test ($n = 3$). *G*) The process of myoblast fusion has been analyzed in C2C12 cells transfected with si8 and phGDNF, or si8 alone or with its mismatched control (M8), after 3 d of differentiation. Values (means ± SEM) are given as the percentage of the fusion index measured in M8 (control) transfected cells. ***$P < 0.001$ and *$P < 0.05$, Bonferroni's multiple comparison test ($n = 3$).

not affected by the absence of APP. Strikingly, APP-dependent *GDNF* transcription does not require AICD release by the γ-secretase and is not regulated by the intracellular domain of APP. The studies of APP-dependent gene transcription were initiated by the observation that the AICD released by γ-secretase cleavage stimulates gene transcription in a heterologous reporter system (7, 8). It established the proof of concept that APP can directly control gene transcription, but did not allow identifying the endogenously regulated genes. Numerous studies have produced controversial results about the identity of APP target genes (10, 31–33), but also about the pathways involved in APP nuclear signaling, and especially whether they rely or not on AICD release (34, 35). We first showed that GDNF levels were significantly restored in APP$^{-/-}$ MEFs stably reexpressing APP751 isoform, but not by APP695. APP751 is the major peripheral and predominant isoform in MEFs and in muscles, whereas there are no detectable levels of the neuronal isoform APP695 in these cells (Supplemental Fig. S4). This observation adds experimental evidence to the hypothesis that differential splicing of APP can contribute to functional diversity (4). Many studies have reported that APP target genes are transcriptionally regulated by the direct binding of AICD to its promoter (10, 36). Important to note, transcriptionally active AICD was reported to be preferentially produced from the amyloidogenic processing of the APP695 isoform (37–39). Our data indicate that APP-dependent GDNF transcription is not relying on AICD by the γ-secretase and, moreover, that APP751 isoforms lacking the C-terminal

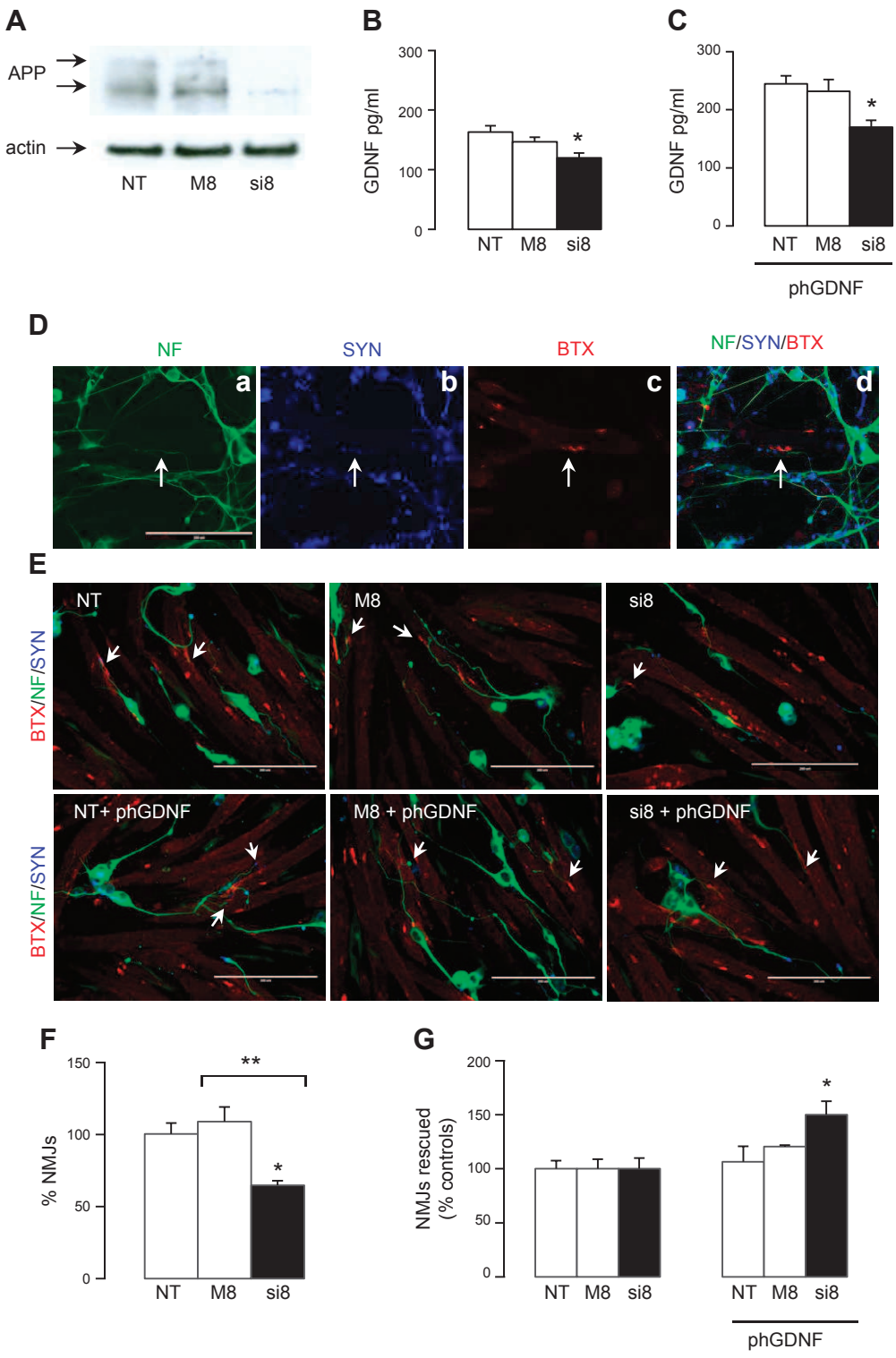

Figure 7. Regulation of GDNF by APP controls NM contacts. Experiments were performed on differentiated C2C12 (muscle cells) and NG108-15 (neuronal cells) cocultures. *A*) The efficiency of APP silencing in C2C12 muscle cells was monitored at the end of the coculture when the formation of NM contacts was analyzed. Western blotting against APP was performed on cell lysates with the 22C11 antibody; actin was used as a protein loading control. *B*) GDNF production was measured by ELISA in the medium of cocultures silenced (si8) or not (NT, M8) for APP and (*C*) transfected or not with the phGDNF expression vector. Results (means ± SEM) are the concentration in picograms per milliliter of GDNF in the culture medium compared to nontransfected (NT) controls. $*P < 0.05$, Bonferroni's multiple comparison test ($n = 4$). *D*) Single channels indicate the labeling of neurons in green (*a*, NF), ACh vesicles in blue (*b*, SYN), and AChRs in red (*c*, BTX), merged in (*d*). An NM contact is defined by the colocalization of the 3 markers, as indicated by the white arrows. *E*) NM contacts formed in each experimental condition were counted per field containing an equivalent number of nerve and muscle cells (*F*). Results are given as the percentage (%) of NM contacts counted in control condition (NT, nontransfected) or as indicated. $*P < 0.05$ and $**P < 0.01$, Bonferroni's multiple comparison test ($n = 4$). *G*) Similar quantifications were performed on cultures with muscle cells transfected by the phGDNF expression plasmid. $*P < 0.05$, Bonferroni's multiple comparison test ($n = 3$).

region restore GDNF expression to a same extent than native APP751. *GDNF* might thus belong to another set of APP target genes, like the acetylcholinesterase gene, which is transcriptionally regulated by APP in an AICD-independent manner (40). One possible hypothesis is that APP recruits through its ectodomain or transmembrane region partner protein directly involved in signal transduction. APP has been shown to form homodimers (41, 42) and heterodimers with APLPs (43) as well as with Notch receptors (44). Quite strikingly, crossing mice expressing APP truncated of its C-terminal part with APLP2 null mice results in similar developmental defects as compared with mice doubly deficient in APP and APLP2 (45), suggesting that APP-APLP2 interactions in APP-dependent signaling might be of primary importance.

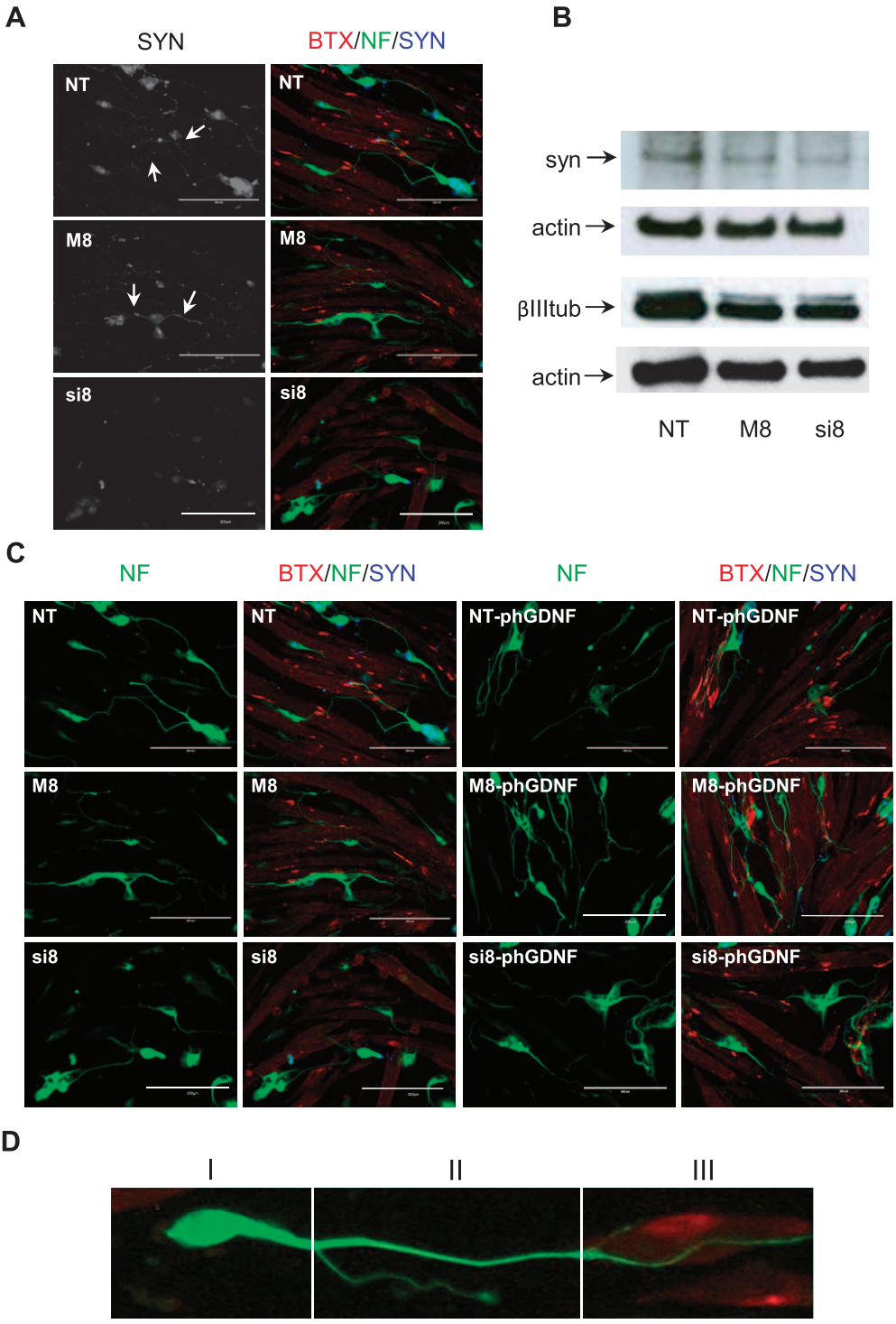

Figure 8. APP-dependent GDNF regulation influences ACh vesicle distribution. Experiments were performed on differentiated C2C12 (muscle cells) and NG-108 (neuronal cells) cocultures. *A*) SYN staining (left panels) in NT, M8, or si8 cocultures and (*B*) SYN protein levels measured by Western blotting performed on coculture cell lysates and compared to βIIItub (neuronal marker) levels. Actin was used as a loading marker to normalize SYN and βIIItub levels. Blots shown are representative of 3 separate experiments. *C*) Morphology of neuronal outgrowths was studied by βIIItub staining (NF) in cocultures where APP expression has been silenced (si8) or not (M8) in muscle cells. Images shown are typical of 6 separate experiments. *D*) A typical image of a differentiated NG108-15 neuron that presents primary (I), secondary (II), and tertiary (III) branches.

Another important question in the field of APP-dependent gene transcription is how APP target gene expression can be related to its function. The phenotype of $APP^{-/-}$ mice is quite silent with the exception of reduced grip strength (Supplemental Fig. S2) and locomotor activity (12, 13). The NM system appears therefore as the best model to investigate the involvement of target genes in APP function (15, 43).We showed that *GDNF* is significantly down-regulated in skeletal muscles from hindlimbs of $APP^{-/-}$, but it is not detectable in neuronal cell cultures and not produced by the cholinergic NG108-15 neuronal cell line (data not shown). GDNF is indeed highly produced by muscles and Schwann cells (18, 19). GDNF heterozygous mice ($^{+/-}$) exhibit locomotor deficiencies (46, 47), suggesting that GDNF dosage plays a key role in NM function. We found that GDNF and APP levels increase in parallel during muscle cell differentiation, and GDNF expression accelerates cell fusion, whereas APP silencing halves the process of muscular differentiation. APP deficiency induced a decrease in muscular GDNF production

TABLE 1. *APP-dependent GDNF regulation influences neuronal maturation*

Branch	NT	M8	Si8	NT plus phGDNF	M8 plus phGDNF	Si8 plus phGDNF
Primary	92 ± 2.8	77 ± 2.2	73 ± 2.7	112 ± 2.8	123 ± 4.3	108 ± 2.5
Secondary	24 ± 2.6	18 ± 1.4	27 ± 2.1	42 ± 2.6	40 ± 2.6	52 ± 2.4
Tertiary	2 ± 0.4	2 ± 0.5	0 ± 0	7 ± 0.9	6 ± 0.6	8 ± 1.6

Neuronal maturation was measured in cocultures after APP silencing (si8) or not (M8) in muscle cells (see Fig. 7*C*) by counting primary, secondary, and tertiary branches with the ImageJ software. The data (percentage) refer to the number of neurons presenting primary, secondary, and tertiary branches on a total of 30 neurons counted per experimental condition. Data were collected from 3 separate experiments ($n = 3$).

and was associated with muscle atrophy *in vivo* and impairment of muscle cell differentiation *in vitro*. Indeed, lower muscle strength observed in $APP^{-/-}$ mice could be due to the decrease of fiber diameter associated or not with a switch of fiber type, from glycolytic muscle fibers exerting high contraction with short duration to smaller oxidative fibers with sustained low contraction. Our *in vitro* data indicate that GDNF promotes muscle cell differentiation into myotubes. Whether GDNF deficiency is involved in the change of muscle morphology observed in $APP^{-/-}$ remains to be firmly established. Nevertheless, our observations suggest that the NM phenotype observed in $APP^{-/-}$ mice results not only from a defect in the neuronal presynaptic compartment but also in impaired muscle differentiation and maintenance associated with decreased GDNF production by muscles themselves.

Recent studies have evidenced a defect of NMJs at the presynaptic compartment in $APP^{-/-}$ and $APLP2^{-/-}$ mice (15, 48). In our work, in line with previous studies (48, 49), $APP^{-/-}$ mice showed an important decrease in ACh vesicle density during NMJ maturation. We also observed this defect at 2 mo, providing here data that were not accessible in APP/APLP2 combined with KO due to early postnatal lethality (15). The absence of APP did not significantly alter the innervation pattern at the NMJ but essentially decreased the marker of synaptic transmission and the clustering of postsynaptic densities. This defect in presynaptic morphology at the NMJ is different from those observed in denervation, where retraction of nerve terminal and fragmentation of postsynaptic densities appear. This profile is more compatible with the reported defect in cholinergic synaptic transmission induced by loss of APP (50).

Neurotrophic factors released from the target are known to modulate the establishment and maintenance of active synapses. GDNF was reported to regulate the postsynaptic insertion, distribution, and stabilization of the AChRs on skeletal muscles (51), but also presynaptic branching and synaptic remodeling (21). In order to get more insight into the involvement of GDNF in APP-dependent NMJ impairments, we set up an *in vitro* model by cultivating differentiated cholinergic neuronal cells on muscle cells. The model does not fully recreate the NMJs but recapitulates some essential features and particularly allows monitoring the establishment of NM contacts by the colocalization of nerve terminal, presynaptic vesicle, and postsynaptic AChR markers (23). Muscular APP silencing in cocultures induced a significant decrease in the GDNF-secreted levels and NM contacts. In muscular APP-silenced cocultures, ACh vesicle density and protein levels were reduced at nerve terminals, whereas neuronal abundance was not altered, consistent with the *in vivo* results. However, neuronal maturation and complexity were affected by muscular APP silencing in our model. Axonal-like processes were significantly shorter and never showed tertiary specialization in APP-silenced conditions. These impairments were rescued by increasing GDNF expression in muscles. The molecular mechanisms underlying this process appear as complex. Retrograde transport of GDNF to neuron cell body is an important step in its function as a trophic factor (18–20). GDNF receptors consist of receptor tyrosine kinase (52) and its preferential ligand-binding protein, the glial cell line-derived neurotrophic factor family receptor subtype 1 (GFRα1) (53). Very importantly, GDNF/GFRα1 promotes *trans*-synaptic adhesion and presynaptic differentiation by directly activating a neural cell adhesion molecule-dependent signaling pathway (54). Strikingly, GDNF-positive effects were significant in APP-silenced cultures, but not in controls, suggesting that the formation of contacts (recapitulating features of NMJs) between neurons and muscle cells is driven by the APP/GDNF interplay rather than GDNF levels *per se*.

One important question is to understand how these observations are relevant to the mechanisms underlying the formation of functional NMJs. Our data indicated that GDNF is able to correct the aberrant presynaptic morphology observed in $APP^{-/-}$ mice. Overexpression of GDNF by muscle was shown to increase the number of motor axons innervating NMJs in neonatal mice (22). Long-term administration of circulating GDNF induces multiple innervations of muscle fibers and continuous remodeling of synapse (21). Our data indicated that when a factor controlling GDNF supply at the NMJ is deficient, the impairment observed can be corrected by GDNF levels. We do not exclude here that APP can also contribute, as it has been reported, by transdimerization with APLPs to anchor the presynaptic and postsynaptic compartments (14, 38). The mechanisms by which APP, partner proteins like LRP4, GDNF, and its receptors cooperate to establish and maintain NMJs need to be further elucidated. For instance, it would be of prime interest to elucidate if the NM phenotype of $APP^{-/-}$ mice primarily results from abnormal muscle physiology, or if the modification of the muscle fibers that we identified in $APP^{-/-}$ mice is a consequence of aberrant NMJs (55).

Understanding the main physiologic role of APP is also of immediate relevance for the comprehension of several pathologies, primarily AD. Importantly, decreases in circulating GDNF levels have been observed in nonbiased studies carried out in AD patient blood and cerebrospinal

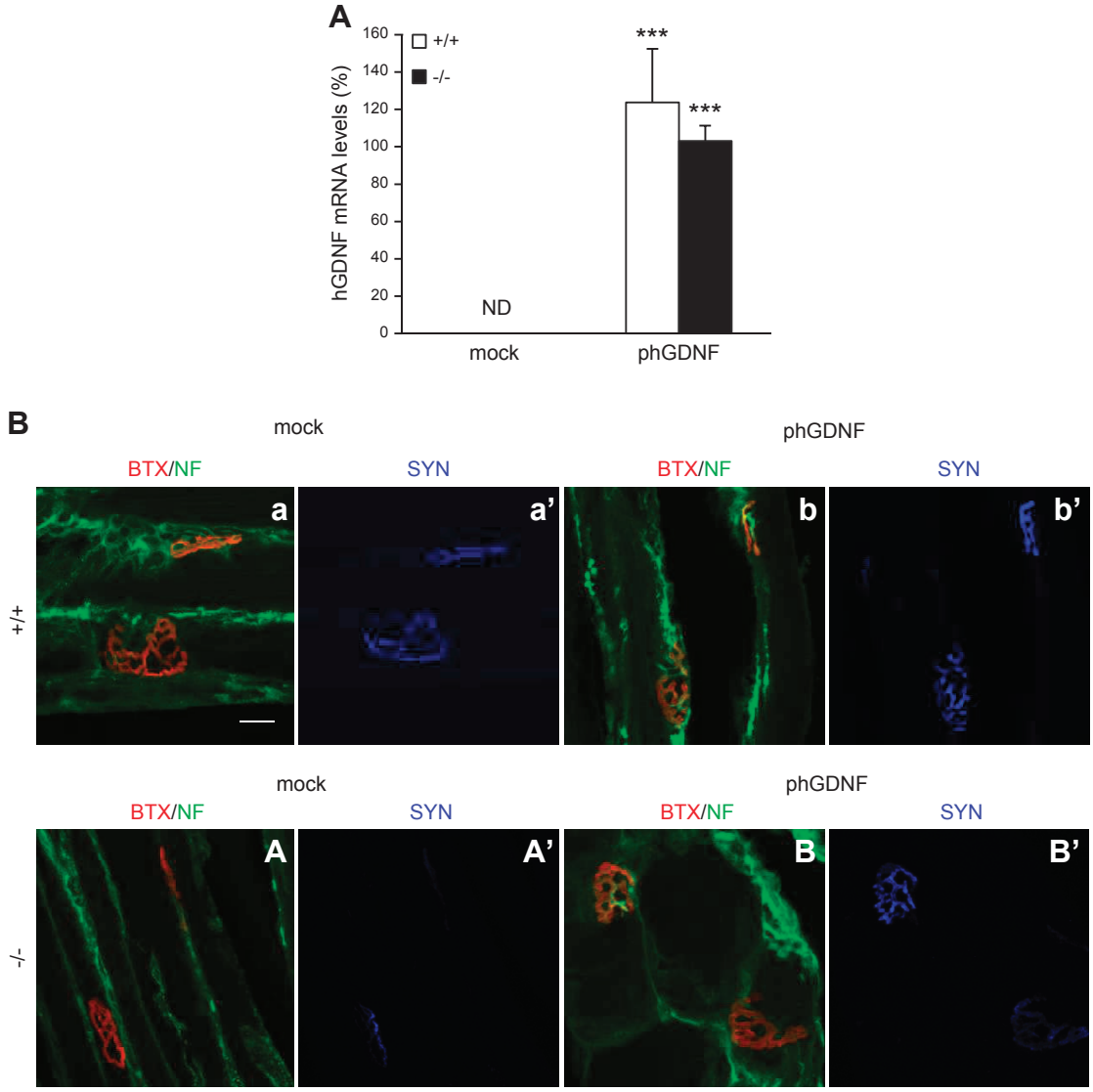

Figure 9. *In vivo* GDNF electroporation restores motor end plate maturation and ACh vesicle distribution in APP$^{-/-}$ mice. *A*) A plasmid coding for phGDNF and the mock were delivered by electroporation of the tibialis muscle in 3-wk-old mice ($n = 4$ per group). phGDNF expression was checked in muscles 10 d after electroporation. Values (means ± SEM) were measured in mock and phGDNF-electroporated tibialis. ***$P < 0.001$, Bonferroni's multiple comparison test ($n = 4$). *B*) Experiments were done on hindlimb sections of APP$^{+/+}$ or APP$^{-/-}$ mice 10 d after electroporation with the empty vector (mock) and the phGDNF. Stainings of pre- and postsynaptic compartments have been analyzed by confocal microscopy to generate z-stack images. Scale bar, 5 μm. *a*–*B*′) Labeling of AChRs with BTX in red, immunofluorescence detection of NF in green, and of SYN in blue. Typical images are shown for each group.

fluid samples (56, 57), identifying GDNF as an AD biomarker. Very recently, it has been shown that in AD, neuron deficiency of GDNF receptor GFRα1 resulted in neuronal death (58). Our study strongly suggests that this pathologic pathway involving GDNF could be directly linked to the physiopathologic role of APP in AD. Growing evidence indicates that defects in APP function might also be directly related to other diseases. APP up-regulation in muscle from patients with amyotrophic lateral sclerosis (ALS) and in the mouse model of familial ALS is correlated with clinical symptoms (59, 60). To note, changes in GDNF levels have also been involved in ALS (61). Increased levels of APP have also been detected in the muscles of patients with another type of muscle disease: inclusion-body myositis (62). Mice with targeted overexpression of APP in skeletal muscle developed histopathologic and clinical features characteristic of inclusion-body myositis, including inflammation and deficiencies in motor performance (63). Our results add evidence to the involvement of APP in neuromuscular pathologies and suggest further analysis of the role of GDNF in these contexts and to evaluate it as a possible target for treatments. FJ

The authors are grateful to Bart de Strooper (Katholieke Universiteit Leuven, Leuven, Belgium) for the kind gift of mouse embryonic fibroblast cells. The authors kindly acknowledge Laetitia El Haylani (Alzheimer Research Group, Université Catholique de Louvain, Institute of Neuroscience, Brussels, Belgium) for her skillful technical assistance. This work was supported by a grant from the Belgian Fonds National pour la Recherche Scientifique (to S.S.), by the S.A.O./F.R.A. Stichting

voor Alzheimer Onderzoek/Foundation for Research on Alzheimer's disease (to P.K.-C.), Interuniversity Attraction Pole Programme-Belgian Sate-Belgian Science Policy (IAP-P7/16 and IAP-P7/13 to J.-N.O., P.K.-C., and P.G.), Fondation Médicale Reine Elisabeth (to J.-N.O., I.D., and P.K.-C.), and Action de Recherche Concertée (14/19-059 to P.K.-C.). F.C. is a research associate, and N.Z. is a postdoctoral researcher of the Belgian Fonds National pour la Recherche Scientifique.

REFERENCES

1. Kang, J., Lemaire, H. G., Unterbeck, A., Salbaum, J. M., Masters, C. L., Grzeschik, K. H., Multhaup, G., Beyreuther, K., and Müller-Hill, B. (1987) The precursor of Alzheimer's disease amyloid A4 protein resembles a cell-surface receptor. *Nature* **325**, 733–736
2. Haass, C., and Selkoe, D. J. (1993) Cellular processing of beta-amyloid precursor protein and the genesis of amyloid beta-peptide. *Cell* **75**, 1039–1042
3. Wasco, W., Bupp, K., Magendantz, M., Gusella, J. F., Tanzi, R. E., and Solomon, F. (1992) Identification of a mouse brain cDNA that encodes a protein related to the Alzheimer disease-associated amyloid beta protein precursor. *Proc. Natl. Acad. Sci. USA* **89**, 10758–10762
4. Shariati, S. A., and De Strooper, B. (2013) Redundancy and divergence in the amyloid precursor protein family. *FEBS Lett.* **587**, 2036–2045
5. Nalivaeva, N. N., and Turner, A. J. (2013) The amyloid precursor protein: a biochemical enigma in brain development, function and disease. *FEBS Lett.* **587**, 2046–2054
6. Ring, S., Weyer, S. W., Kilian, S. B., Waldron, E., Pietrzik, C. U., Filippov, M. A., Herms, J., Buchholz, C., Eckman, C. B., Korte, M., Wolfer, D. P., and Müller, U. C. (2007) The secreted beta-amyloid precursor protein ectodomain APPs alpha is sufficient to rescue the anatomical, behavioral, and electrophysiological abnormalities of APP-deficient mice. *J. Neurosci.* **27**, 7817–7826
7. Cao, X., and Südhof, T. C. (2001) A transcriptionally [correction of transcriptively] active complex of APP with Fe65 and histone acetyltransferase Tip60. *Science* **293**, 115–120
8. Cao, X., and Südhof, T. C. (2004) Dissection of amyloid-beta precursor protein-dependent transcriptional transactivation. *J. Biol. Chem.* **279**, 24601–24611
9. Huysseune, S., Kienlen-Campard, P., Hébert, S., Tasiaux, B., Leroy, K., Devuyst, O., Brion, J. P., De Strooper, B., and Octave, J. N. (2009) Epigenetic control of aquaporin 1 expression by the amyloid precursor protein. *FASEB J.* **23**, 4158–4167
10. Pardossi-Piquard, R., Petit, A., Kawarai, T., Sunyach, C., Alves da Costa, C., Vincent, B., Ring, S., D'Adamio, L., Shen, J., Müller, U., St George Hyslop, P., and Checler, F. (2005) Presenilin-dependent transcriptional control of the Abeta-degrading enzyme neprilysin by intracellular domains of betaAPP and APLP. *Neuron* **46**, 541–554
11. Nalivaeva, N. N., Belyaev, N. D., Zhuravin, I. A., and Turner, A. J. (2012) The Alzheimer's amyloid-degrading peptidase, neprilysin: can we control it? *Int. J. Alzheimers Dis.* **2012**, 383796
12. Zheng, H., Jiang, M., Trumbauer, M. E., Sirinathsinghji, D. J., Hopkins, R., Smith, D. W., Heavens, R. P., Dawson, G. R., Boyce, S., Conner, M. W., Stevens, K. A., Slunt, H. H., Sisoda, S. S., Chen, H. Y., and Van der Ploeg, L. H. (1995) beta-Amyloid precursor protein-deficient mice show reactive gliosis and decreased locomotor activity. *Cell* **81**, 525–531
13. Müller, U., Cristina, N., Li, Z. W., Wolfer, D. P., Lipp, H. P., Rülicke, T., Brandner, S., Aguzzi, A., and Weissmann, C. (1994) Behavioral and anatomical deficits in mice homozygous for a modified beta-amyloid precursor protein gene. *Cell* **79**, 755–765
14. Caldwell, J. H., Klevanski, M., Saar, M., and Müller, U. C. (2013) Roles of the amyloid precursor protein family in the peripheral nervous system. *Mech. Dev.* **130**, 433–446
15. Klevanski, M., Saar, M., Baumkötter, F., Weyer, S. W., Kins, S., and Müller, U. C. (2014) Differential role of APP and APLPs for neuromuscular synaptic morphology and function. *Mol. Cell. Neurosci.* **61**, 201–210
16. Lin, L. F., Doherty, D. H., Lile, J. D., Bektesh, S., and Collins, F. (1993) GDNF: a glial cell line-derived neurotrophic factor for midbrain dopaminergic neurons. *Science* **260**, 1130–1132
17. Caumont, A. S., Octave, J. N., and Hermans, E. (2006) Specific regulation of rat glial cell line-derived neurotrophic factor gene expression by riluzole in C6 glioma cells. *J. Neurochem.* **97**, 128–139
18. Suzuki, H., Hase, A., Miyata, Y., Arahata, K., and Akazawa, C. (1998) Prominent expression of glial cell line-derived neurotrophic factor in human skeletal muscle. *J. Comp. Neurol.* **402**, 303–312
19. Nagano, M., and Suzuki, H. (2003) Quantitative analyses of expression of GDNF and neurotrophins during postnatal development in rat skeletal muscles. *Neurosci. Res.* **45**, 391–399
20. Trupp, M., Rydén, M., Jörnvall, H., Funakoshi, H., Timmusk, T., Arenas, E., and Ibáñez, C. F. (1995) Peripheral expression and biological activities of GDNF, a new neurotrophic factor for avian and mammalian peripheral neurons. *J. Cell Biol.* **130**, 137–148
21. Keller-Peck, C. R., Feng, G., Sanes, J. R., Yan, Q., Lichtman, J. W., and Snider, W. D. (2001) Glial cell line-derived neurotrophic factor administration in postnatal life results in motor unit enlargement and continuous synaptic remodeling at the neuromuscular junction. *J. Neurosci.* **21**, 6136–6146
22. Nguyen, Q. T., Parsadanian, A. S., Snider, W. D., and Lichtman, J. W. (1998) Hyperinnervation of neuromuscular junctions caused by GDNF overexpression in muscle. *Science* **279**, 1725–1729
23. Vianney, J. M., and Spitsbergen, J. M. (2011) Cholinergic neurons regulate secretion of glial cell line-derived neurotrophic factor by skeletal muscle cells in culture. *Brain Res.* **1390**, 1–9
24. Senechal, Y., Kelly, P. H., Cryan, J. F., Natt, F., and Dev, K. K. (2007) Amyloid precursor protein knockdown by siRNA impairs spontaneous alternation in adult mice. *J. Neurochem.* **102**, 1928–1940
25. Zanou, N., Shapovalov, G., Louis, M., Tajeddine, N., Gallo, C., Van Schoor, M., Anguish, I., Cao, M. L., Schakman, O., Dietrich, A., Lebacq, J., Ruegg, U., Roulet, E., Birnbaumer, L., and Gailly, P. (2010) Role of TRPC1 channel in skeletal muscle function. *Am. J. Physiol. Cell Physiol.* **298**, C149–C162
26. Ducret, T., Vandebrouck, C., Cao, M. L., Lebacq, J., and Gailly, P. (2006) Functional role of store-operated and stretch-activated channels in murine adult skeletal muscle fibres. *J. Physiol.* **575**, 913–924
27. Audouard, E., Schakman, O., René, F., Huettl, R. E., Huber, A. B., Loeffler, J. P., Gailly, P., and Clotman, F. (2012) The Onecut transcription factor HNF-6 regulates in motor neurons the formation of the neuromuscular junctions. *PLoS One* **7**, e50509
28. Vandermeulen, G., Staes, E., Vanderhaeghen, M. L., Bureau, M. F., Scherman, D., and Préat, V. (2007) Optimisation of intradermal DNA electrotransfer for immunisation. *J. Control. Release* **124**, 81–87
29. Bloquel, C., Fabre, E., Bureau, M. F., and Scherman, D. (2004) Plasmid DNA electrotransfer for intracellular and secreted proteins expression: new methodological developments and applications. *J. Gene Med.* **6** (Suppl 1), S11–S23
30. Wong, S. H., Lowes, K. N., Quigley, A. F., Marotta, R., Kita, M., Byrne, E., Kornberg, A. J., Cook, M. J., and Kapsa, R. M. (2005) DNA electroporation in vivo targets mature fibres in dystrophic mdx muscle. *Neuromuscul. Disord.* **15**, 630–641
31. Baek, S. H., Ohgi, K. A., Rose, D. W., Koo, E. H., Glass, C. K., and Rosenfeld, M. G. (2002) Exchange of N-CoR corepressor and Tip60 coactivator complexes links gene expression by NF-kappaB and beta-amyloid precursor protein. *Cell* **110**, 55–67
32. Hébert, S. S., Serneels, L., Tolia, A., Craessaerts, K., Derks, C., Filippov, M. A., Müller, U., and De Strooper, B. (2006) Regulated intramembrane proteolysis of amyloid precursor protein and regulation of expression of putative target genes. *EMBO Rep.* **7**, 739–745
33. Von Rotz, R. C., Kohli, B. M., Bosset, J., Meier, M., Suzuki, T., Nitsch, R. M., and Konietzko, U. (2004) The APP intracellular domain forms nuclear multiprotein complexes and regulates the transcription of its own precursor. *J. Cell Sci.* **117**, 4435–4448
34. Waldron, E., Isbert, S., Kern, A., Jaeger, S., Martin, A. M., Hébert, S. S., Behl, C., Weggen, S., De Strooper, B., and Pietrzik, C. U. (2008) Increased AICD generation does not result in increased nuclear translocation or activation of target gene transcription. *Exp. Cell Res.* **314**, 2419–2433
35. Beckett, C., Nalivaeva, N. N., Belyaev, N. D., and Turner, A. J. (2012) Nuclear signalling by membrane protein intracellular domains: the AICD enigma. *Cell. Signal.* **24**, 402–409
36. Belyaev, N. D., Nalivaeva, N. N., Makova, N. Z., and Turner, A. J. (2009) Neprilysin gene expression requires binding of the amyloid precursor protein intracellular domain to its promoter: implications for Alzheimer disease. *EMBO Rep.* **10**, 94–100
37. Belyaev, N. D., Kellett, K. A., Beckett, C., Makova, N. Z., Revett, T. J., Nalivaeva, N. N., Hooper, N. M., and Turner, A. J. (2010) The

transcriptionally active amyloid precursor protein (APP) intracellular domain is preferentially produced from the 695 isoform of APP in a beta-secretase-dependent pathway. *J. Biol. Chem.* **285**, 41443–41454
38. Goodger, Z. V., Rajendran, L., Trutzel, A., Kohli, B. M., Nitsch, R. M., and Konietzko, U. (2009) Nuclear signaling by the APP intracellular domain occurs predominantly through the amyloidogenic processing pathway. *J. Cell Sci.* **122**, 3703–3714
39. Flammang, B., Pardossi-Piquard, R., Sevalle, J., Debayle, D., Dabert-Gay, A. S., Thévenet, A., Lauritzen, I., and Checler, F. (2012) Evidence that the amyloid-β protein precursor intracellular domain, AICD, derives from β-secretase-generated C-terminal fragment. *J. Alzheimers Dis.* **30**, 145–153
40. Hicks, D. A., Makova, N. Z., Gough, M., Parkin, E. T., Nalivaeva, N. N., and Turner, A. J. (2013) The amyloid precursor protein represses expression of acetylcholinesterase in neuronal cell lines. *J. Biol. Chem.* **288**, 26039–26051
41. Ben Khalifa, N., Tyteca, D., Marinangeli, C., Depuydt, M., Collet, J. F., Courtoy, P. J., Renauld, J. C., Constantinescu, S., Octave, J. N., and Kienlen-Campard, P. (2012) Structural features of the KPI domain control APP dimerization, trafficking, and processing. *FASEB J.* **26**, 855–867
42. Decock, M., El Haylani, L., Stanga, S., Dewachter, I., Octave, J. N., Smith, S. O., Constantinescu, S. N., and Kienlen-Campard, P. (2015) Analysis by a highly sensitive split luciferase assay of the regions involved in APP dimerization and its impact on processing. *FEBS Open Bio* **5**, 763–773
43. Soba, P., Eggert, S., Wagner, K., Zentgraf, H., Siehl, K., Kreger, S., Löwer, A., Langer, A., Merdes, G., Paro, R., Masters, C. L., Müller, U., Kins, S., and Beyreuther, K. (2005) Homo- and heterodimerization of APP family members promotes intercellular adhesion. *EMBO J.* **24**, 3624–3634
44. Chen, C. D., Oh, S. Y., Hinman, J. D., and Abraham, C. R. (2006) Visualization of APP dimerization and APP-Notch2 heterodimerization in living cells using bimolecular fluorescence complementation. *J. Neurochem.* **97**, 30–43
45. Li, H., Wang, Z., Wang, B., Guo, Q., Dolios, G., Tabuchi, K., Hammer, R. E., Südhof, T. C., Wang, R., and Zheng, H. (2010) Genetic dissection of the amyloid precursor protein in developmental function and amyloid pathogenesis. *J. Biol. Chem.* **285**, 30598–30605
46. Boger, H. A., Middaugh, L. D., Huang, P., Zaman, V., Smith, A. C., Hoffer, B. J., Tomac, A. C., and Granholm, A. C. (2006) A partial GDNF depletion leads to earlier age-related deterioration of motor function and tyrosine hydroxylase expression in the substantia nigra. *Exp. Neurol.* **202**, 336–347
47. Littrell, O. M., Pomerleau, F., Huettl, P., Surgener, S., McGinty, J. F., Middaugh, L. D., Granholm, A. C., Gerhardt, G. A., and Boger, H. A. (2012) Enhanced dopamine transporter activity in middle-aged Gdnf heterozygous mice. *Neurobiol. Aging* **33**, 427.e1–427.e14
48. Wang, P., Yang, G., Mosier, D. R., Chang, P., Zaidi, T., Gong, Y. D., Zhao, N. M., Dominguez, B., Lee, K. F., Gan, W. B., and Zheng, H. (2005) Defective neuromuscular synapses in mice lacking amyloid precursor protein (APP) and APP-Like protein 2. *J. Neurosci.* **25**, 1219–1225
49. Wang, Z., Wang, B., Yang, L., Guo, Q., Aithmitti, N., Songyang, Z., and Zheng, H. (2009) Presynaptic and postsynaptic interaction of the amyloid precursor protein promotes peripheral and central synaptogenesis. *J. Neurosci.* **29**, 10788–10801
50. Wang, B., Yang, L., Wang, Z., and Zheng, H. (2007) Amyolid precursor protein mediates presynaptic localization and activity of the high-affinity choline transporter. *Proc. Natl. Acad. Sci. USA* **104**, 14140–14145
51. Yang, L. X., and Nelson, P. G. (2004) Glia cell line-derived neurotrophic factor regulates the distribution of acetylcholine receptors in mouse primary skeletal muscle cells. *Neuroscience* **128**, 497–509
52. Treanor, J. J., Goodman, L., de Sauvage, F., Stone, D. M., Poulsen, K. T., Beck, C. D., Gray, C., Armanini, M. P., Pollock, R. A., Hefti, F., Phillips, H. S., Goddard, A., Moore, M. W., Buj-Bello, A., Davies, A. M., Asai, N., Takahashi, M., Vandlen, R., Henderson, C. E., and Rosenthal, A. (1996) Characterization of a multicomponent receptor for GDNF. *Nature* **382**, 80–83
53. Sariola, H., and Saarma, M. (2003) Novel functions and signalling pathways for GDNF. *J. Cell Sci.* **116**, 3855–3862
54. Ledda, F., Paratcha, G., Sandoval-Guzmán, T., and Ibáñez, C. F. (2007) GDNF and GFRalpha1 promote formation of neuronal synapses by ligand-induced cell adhesion. *Nat. Neurosci.* **10**, 293–300
55. Tintignac, L. A., Brenner, H. R., and Rüegg, M. A. (2015) Mechanisms regulating neuromuscular junction development and function and causes of muscle wasting. *Physiol. Rev.* **95**, 809–852
56. Ray, S., Britschgi, M., Herbert, C., Takeda-Uchimura, Y., Boxer, A., Blennow, K., Friedman, L. F., Galasko, D. R., Jutel, M., Karydas, A., Kaye, J. A., Leszek, J., Miller, B. L., Minthon, L., Quinn, J. F., Rabinovici, G. D., Robinson, W. H., Sabbagh, M. N., So, Y. T., Sparks, D. L., Tabaton, M., Tinklenberg, J., Yesavage, J. A., Tibshirani, R., and Wyss-Coray, T. (2007) Classification and prediction of clinical Alzheimer's diagnosis based on plasma signaling proteins. *Nat. Med.* **13**, 1359–1362
57. Straten, G., Eschweiler, G. W., Maetzler, W., Laske, C., and Leyhe, T. (2009) Glial cell-line derived neurotrophic factor (GDNF) concentrations in cerebrospinal fluid and serum of patients with early Alzheimer's disease and normal controls. *J. Alzheimers Dis.* **18**, 331–337
58. Konishi, Y., Yang, L. B., He, P., Lindholm, K., Lu, B., Li, R., and Shen, Y. (2014) Deficiency of GDNF receptor GFRα1 in Alzheimer's neurons results in neuronal death. *J. Neurosci.* **34**, 13127–13138
59. Bryson, J. B., Hobbs, C., Parsons, M. J., Bosch, K. D., Pandraud, A., Walsh, F. S., Doherty, P., and Greensmith, L. (2012) Amyloid precursor protein (APP) contributes to pathology in the SOD1 (G93A) mouse model of amyotrophic lateral sclerosis. *Hum. Mol. Genet.* **21**, 3871–3882
60. Koistinen, H., Prinjha, R., Soden, P., Harper, A., Banner, S. J., Pradat, P. F., Loeffler, J. P., and Dingwall, C. (2006) Elevated levels of amyloid precursor protein in muscle of patients with amyotrophic lateral sclerosis and a mouse model of the disease. *Muscle Nerve* **34**, 444–450
61. Lie, D. C., and Weis, J. (1998) GDNF expression is increased in denervated human skeletal muscle. *Neurosci. Lett.* **250**, 87–90
62. Askanas, V., and Engel, W. K. (2002) Inclusion-body myositis and myopathies: different etiologies, possibly similar pathogenic mechanisms. *Curr. Opin. Neurol.* **15**, 525–531
63. Sugarman, M. C., Yamasaki, T. R., Oddo, S., Echegoyen, J. C., Murphy, M. P., Golde, T. E., Jannatipour, M., Leissring, M. A., and LaFerla, F. M. (2002) Inclusion body myositis-like phenotype induced by transgenic overexpression of beta APP in skeletal muscle. *Proc. Natl. Acad. Sci. USA* **99**, 6334–6339

Received for publication July 9, 2015.
Accepted for publication December 8, 2015.

Figure S1

Genes (Affymetrix®)	Fold induction/repression
	MEF APP+/+ vs MEF APP-/- (mean log ratio, n=2)
GDNF (1419080_at)	3.5 (↑)
Aquaporin 1 (1416203_at)	3.5 (↑)
Neprilysin (1422975_at)	0.45
Fe65 (Apbb1) (1423892_at) (1423893_x_at)	0.35 0.1
Glycogen synthase kinase 3 beta (1451020_at)	0.2
LRP1 (1448655)	-0.55
EGFr (1460420_a_at) (1424932_at)	-0.25 1.6

Figure S1. Micro arrays experiments.
RNA was extracted after 24 h of culture using Tripure Isolation Reagent (Roche Diagnostics) and RNA quality was checked by agarose gel electrophoresis. Biotin) labeled cRNA was prepared from 5 ug of total RNA using the one-cycle target labelling procedure and hybridized to "GeneChip® Mouse GENOME 430A2,0 Array" representing approximately14,000 well-characterized mouse genes which was then scanned on the Gene Array Scanner (Helwlett Packard). Data acquisition and processing were conducted with Affymetrix Micro array Suite 5,0 and Excel. This table presents the levels of expression of GDNF and putative APP target genes in mouse embryonic fibroblasts expressing or not APP (mean of the log ratio, n=2). Genes whose expression ratios differences were over threefold ($p<0,05$) in APP+/+ compared to APP-/- cells are considered as induced (↑) or repressed (↓).

Figure S2

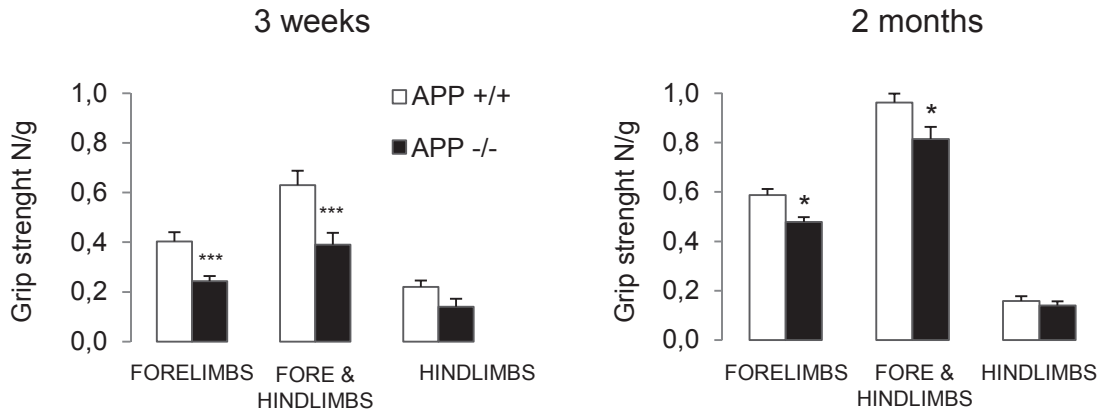

Figure S2. APP-/- mice show impaired grip strength.
APP-/- and control mice (APP+/+) were subjected to a grip-strength test at 3 weeks or 2 months of age. Forelimb as well as the fore and hind limb grip strength were measured with a grip strength meter (San Diego Instruments). Animals held by the tail were positioned horizontally and allowed to place their forepaws and subsequently their fore and hind paws on the grid of the pull bar connected to the force sensor. Mice were slowly pulled away until they loosened the grid. The force applied to the bar, at the moment the grasp was released, was recorded as the peak tension (T-PK). Each non-trained mouse was subjected to three consecutive tests. The maximal force reached by the animal was recorded and absolute strength was normalized to body mass and expressed as newton per gram. The experimenter was blind to genotype. Data (mean ± SEM) are expressed as Newton per grams (N/g body weight) of APP+/+; * $p < 0.5$, *** $p < 0.001$ Bonferroni's multiple comparison test (n= 10 mice).

Figure S3

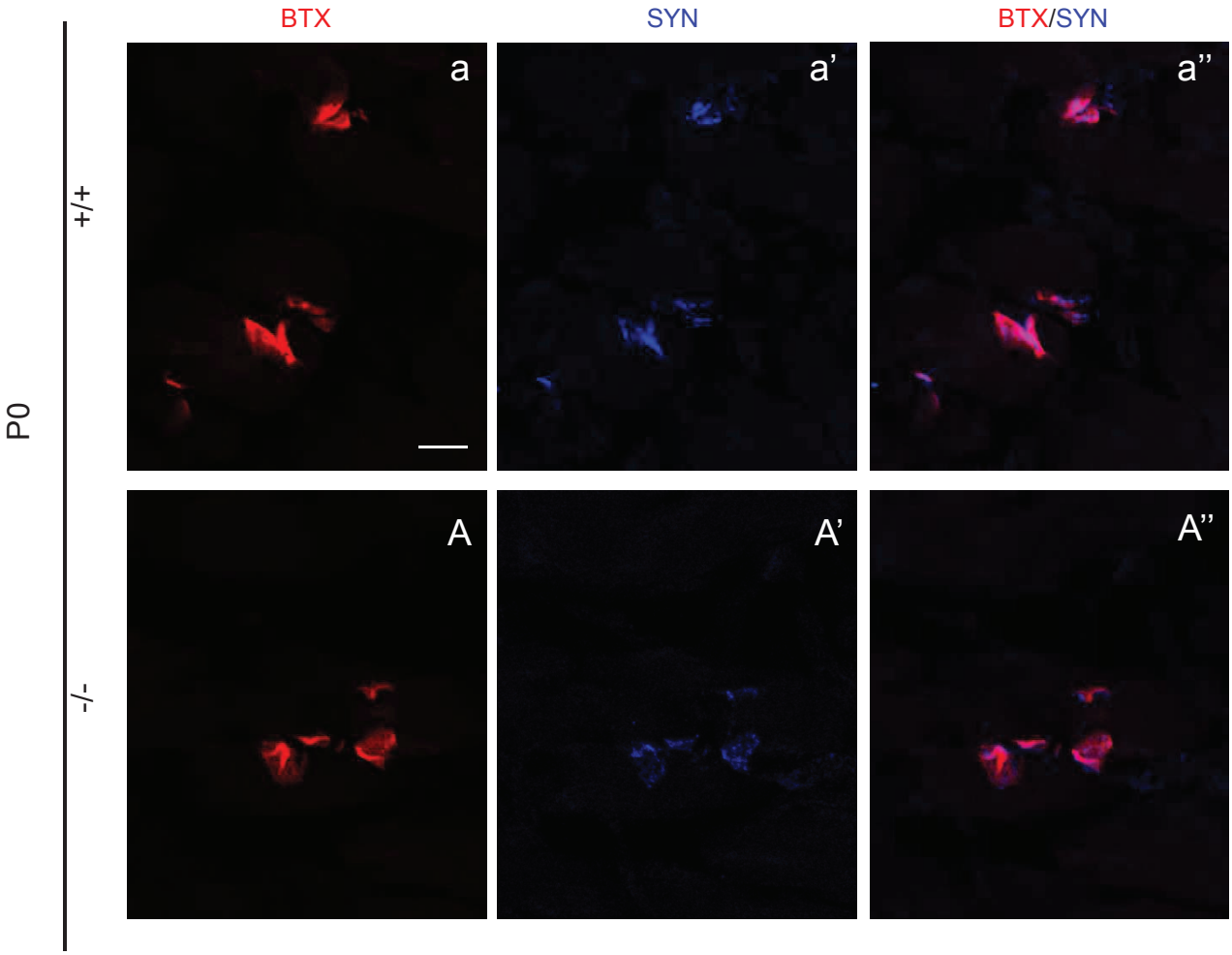

Figure S3. Appropriate nerve and muscular terminals apposition at birth.
Experiments were carried out on hindlimbs sections of APP+/+ or APP-/- mice at birth (P0). Immunohistochemistry of pre- and postsynaptic compartments has been analyzed by confocal microscopy to generate z-stacks images (scale bar 5 µm). (a-A) Labeling of acetylcholine receptors (AchRs) with α-bungarotoxin (BTX) appears in red and immunofluorescence detection of synaptophysin (SYN) in blue (a'-A') and their merge (a''-A''). The totality of NMJs from control and APP-/- mice showed extensive superposition of BTX and of SYN, indicative of precise apposition of motor nerve terminals to the motor endplates at birth.

Figure S4

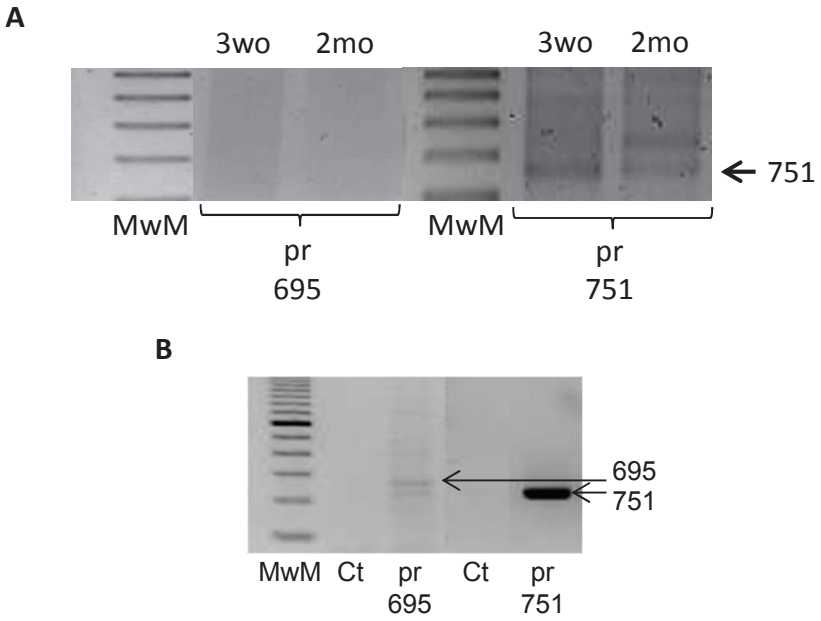

Figure S4. Muscles from APP wild-type mice and MEF cells express APP751 isoform.
RT-PCR analysis of the endogenous APP isoform expressed in muscles and MEF cells. RT-PCR experiments were carried out by using Pfu DNA polymerase (Fermentas) with 2ng/10ml cDNA templates with primers specific for the APP695 (pr695) or the APP751 (pr751) isoforms. DNA amplification products were run on 2% agarose gel and visualized by Midori Green Advance dye under UV light. MWM = Molecular weight marker (0.1 kb). (A) In muscles, as expected, both at 3 weeks or 2 month of age (3wo, 2mo) APP751 is the predominant isoform while there are no detectable levels of APP695. (B) Also in MEF cells APP751 is the predominant isoform with only barely detectable levels of APP695.

The sequences for RT-PCR primers are:
APP695 forward: 5'-GATGAGGATGTGGAGGATG-3'
reverse: 5'-GTCTCTCATTGGCTGCTTCC-3'
APP751 forward: 5'-CCATTTCCAGAAAGCCAAAG-3'
reverse: 5'-TGAGCATGGCTTCAACTCTG-3'